



**University of  
Zurich**<sup>UZH</sup>

# Automated classification of supraglacial surface facies for snow line altitude monitoring using the Google Earth Engine

GEO 511 Master's Thesis

**Author**

Josias Zeller

14-711-238

**Supervised by**

Dr. Hendrik Wulf

Dr. Philipp Rastner

**Faculty representative**

Prof. Dr. Michael Schaepman

30.06.2020

Department of Geography, University of Zurich



**University of  
Zurich<sup>UZH</sup>**

GEO 511  
Master Thesis  
June 30, 2020

**Automated classification of supraglacial surface facies for  
snow line altitude monitoring using the Google Earth  
Engine**

Josias ZELLER  
14-711-238

Supervised by:

Dr. Hendrik WULF

Dr. Philipp RASTNER

Faculty representative:

Prof. Dr. Michael SCHAEPMAN

Remote Sensing Laboratories  
Department of Geography  
University of Zurich



## Abstract

Glaciers represent an important part of the world's freshwater resources used for agriculture and drinking water. Driven by atmospheric warming, most glaciers are losing mass at accelerated rates. Quantifying these changes with mass balances using photogrammetric or ground-based methods can be time-consuming and expensive. To approximate the annual mass balance, the variations in snow cover extent on the glacier can be used instead. Optical satellite imagery facilitates a continuous monitoring of the glacial snow cover and snow line altitude (SLA) during the ablation period. The maximum SLA can be used as an approximation of the Equilibrium Line Altitude (ELA), which is linked to a glacier mass balance.

In the context of this thesis, we developed and validated an application to classify glacier surfaces over time and extract information on snow cover ratio and the snow line altitude. Using a pixel-based analysis of the combined time series from Landsat and Sentinel-2 sensors enables us to monitor glacier changes throughout the ablation phase despite heavy cloud cover.

In a first step, we classify on a given glacier its surface for snow, ice, debris cover, water, clouds and shadows. Based on available referenced data, we validated that we can accurately detect snow surfaces with an overall accuracy from 82 % to 92 %. Subsequently, we developed and validated three approaches to extract the SLA from a given satellite observation. Using independent SLA time series, we could validate that our (a) Histogram, (b) Main Patches and (c) Altitude Bins approaches operate with  $R^2$  accuracies of 0.68, 0.91 and 0.92, respectively.

This thesis highlights the importance of an accurate glacier surface classification for the extraction of the SLA by accounting for its variability of glacier facies. Our developed approaches reveal high accuracies to extract the SLA and the snow cover ratio for an improved approximation of the ELA. As our process is fully automated, it's now possible to extract the SLA history of any given glacier for a selected period of interest over the past decades.



# Contents

<b>Abstract</b>	<b>III</b>
<b>Abbreviations</b>	<b>VII</b>
<b>List of Figures</b>	<b>IX</b>
<b>List of Tables</b>	<b>XI</b>
<b>1 Introduction</b>	<b>1</b>
1.1 Monitoring global glacier change . . . . .	1
1.2 Glacier facies . . . . .	1
1.3 Research objectives . . . . .	2
1.4 Structure of the thesis . . . . .	2
<b>2 Target Areas and Glaciological Background</b>	<b>3</b>
2.1 Target Areas . . . . .	3
2.2 Glaciological background . . . . .	4
2.2.1 Measuring glacier mass balance . . . . .	5
2.2.2 Maximum SLA and ELA . . . . .	5
<b>3 Data</b>	<b>7</b>
3.1 Optical Data . . . . .	7
3.1.1 Landsat 5, 7 and 8 . . . . .	8
3.1.2 Sentinel-2 . . . . .	9
3.2 Digital Elevation Model (DEM) . . . . .	9
3.3 Glacier outlines . . . . .	10
3.4 ELA and AAR Data by the WGMS . . . . .	10
<b>4 Methods</b>	<b>11</b>
4.1 Preparation of Data . . . . .	12
4.1.1 Add Albedo Band . . . . .	12
4.1.2 Cloud filter . . . . .	13
4.2 Classification . . . . .	13
4.2.1 Classes . . . . .	13
4.2.2 Hill Shadow . . . . .	14
4.2.3 Cloud Shadow . . . . .	15

4.2.4	NDWI and NDSI . . . . .	15
4.2.5	Otsu with NIR . . . . .	16
4.3	Random Forest . . . . .	16
4.4	SLA and SCR Extraction . . . . .	17
4.4.1	Main Patches Approach . . . . .	17
4.4.2	Histogram Approach . . . . .	18
4.4.3	Altitude Bin Approach . . . . .	19
4.5	Implementation as a GEE App . . . . .	20
<b>5</b>	<b>Results</b>	<b>23</b>
5.1	Validation of the classification . . . . .	23
5.1.1	Qualitative comparison with ASMAG (Rastner et al., 2019) . . . . .	23
5.1.2	Validation with visually drawn snow cover classifications . . . . .	24
5.2	Validation of the SLA and SCR Extraction . . . . .	26
5.2.1	Snow Cover Ratio Extraction . . . . .	27
5.2.2	Snow Line Altitude Extraction . . . . .	27
5.2.3	Comparison with ELA and AAR-Data from the WGMS . . . . .	29
<b>6</b>	<b>Discussion</b>	<b>33</b>
6.1	Classification of glacial surface facies . . . . .	33
6.1.1	Accuracy of the classification . . . . .	33
6.1.2	Random Forest Classifier . . . . .	34
6.2	Snow Line Altitude and Snow Cover Ratio Extraction . . . . .	35
6.3	DEM Selection and Systematic Bias . . . . .	36
6.4	Monitor the SLA und SCR with a high temporal resolution . . . . .	37
<b>7</b>	<b>Conclusion</b>	<b>39</b>
	<b>Bibliography</b>	<b>41</b>
<b>8</b>	<b>Appendices</b>	<b>45</b>
8.1	Code . . . . .	45
8.2	Data Tables . . . . .	46
	<b>Acknowledgements</b>	<b>49</b>
	<b>Personal Declaration</b>	<b>51</b>

## Abbreviations

AAR	Accumulation-Area Ratio
ALOS	Advanced Land Observing Satellite
ASTER	Advanced Spaceborne Thermal Emission and Reflection Radiometer
BSS	Between Sum of Squares)
CSV	Comma-separated values
DEM	Digital Elevation Model
ELA	Equilibrium-Line Altitude
ESA	European Space Agency
GEE	Google Earth Engine
GUI	Graphical User Interface
JAXA	Japan Aerospace Exploration Agency
m.a.s.l	Meters Above Sea Level
NASA	National Aeronautics and Space Administration
NDSI	Normalized Difference Snow Index
NDWI	Normalized Difference Water Index
NIR	Near Infrared
RF	Random Forest
RGB	Red-Green-Blue
RGI	Randolph Glacier Inventory
SC	Snow Cover
SCA	Snow Covered Area
SCR	Snow Cover Ratio
SLA	Snow Line Altitude
SRTM	Shuttle Radar Topographic Mission
SWIR	Shortwave Infrared
TOA	Top-Of-Atmosphere
VPB	Vertical Mass Balance Profile
VIS	Visible Spectrum
WGMS	World Glacier Monitoring Service





## List of Figures

2.1	Map with all glaciers from the target area . . . . .	3
3.1	Image availability in the Ötztal Alps . . . . .	7
4.1	Architecture of the programm . . . . .	11
4.2	Overview on the modular structure of the program . . . . .	12
4.3	Workflow of the pixelwise classification . . . . .	14
4.4	Workflow of the Random Forest Classifier . . . . .	16
4.5	Example of SLA determination with the Main Patches approach . . . . .	17
4.6	Snow and Ice distribution by altitude for the Histogram approach . . . . .	18
4.7	Example of the Altitude Bin approach . . . . .	19
4.8	Screenshot from the GEE-Application . . . . .	20
5.1	Comparison of snow cover maps 1 . . . . .	24
5.2	Comparison of snow cover maps 2 . . . . .	25
5.3	Snow Cover Comparison with manually digitized Snow Line . . . . .	26
5.4	Validation of the SCR-Values of the Ötztal Alps . . . . .	28
5.5	Validation of the SLA values from the Abramov Glacier . . . . .	30
5.6	Snow Line Altitude from Vernagtferner (2015 to 2019) . . . . .	31
5.7	Snow Cover Ratio from Kesselwandferner (2015 to 2019) . . . . .	31



## List of Tables

2.1	List with all glaciers from the target areas . . . . .	4
3.1	Spectral bands of Landsat 5, 7, 8 and Sentinel-2 . . . . .	8
3.2	Comparison of potential DEM . . . . .	9
4.1	Classes of the classifier . . . . .	15
4.2	Main Patch Approach: Hierarchy of rules applied for SLA extraction . . . . .	17
4.3	Histogram Approach: Hierarchy of rules applied for SLA extraction . . . . .	18
4.4	Altitude Bin approach: Hierarchy of rules applied for SLA extraction . . . . .	19
4.5	Column captions of the export files . . . . .	21
5.1	Cohen's Kappa Interpretation . . . . .	26
5.2	Results of the classification validation . . . . .	27
5.3	Results from the SLA-Validation . . . . .	29
8.1	SCR and SLA from Kesselwandferner 2015 to 2019 . . . . .	46
8.2	SCR and SLA from Vernagtferner 2015 to 2019 . . . . .	47



# 1 Introduction

## 1.1 Monitoring global glacier change

Glaciers are an important source of essential water supplies. Immerzeel et al. (2020) quantify the dependence of natural and human water demand worldwide. Their analysis showed that 22 % of the world's population obtain their water from snow and ice reserves. The proportion of water from snow and ice reserves is highest in the Himalayas (depending on catchment up to 100 % dependence) . In the European Alps the proportion is between 32 % and 45 %, whereby these values refer to the entire hydrological system and locally there can be a massively higher dependence on meltwater.

Glaciers have been losing mass globally for several decades. This glacier recession is driven by the atmospheric warming. The global trend of mass loss is significant. Glaciers worldwide outside Greenland and Antarctica lost mass at an average rate of  $220 \pm 30 \text{ Gt yr}^{-1}$  in 2006–2015 (IPCC, 2019, Zemp et al., 2019). Due to the complex dependence of glaciers on the spatially variable radiation balance and precipitation, it's important to consider interannual and regional variability (Medwedeff and Roe, 2017).

To determine the annual mass balance of a glacier, the equilibrium line is used. The equilibrium line altitude (ELA) indicates the elevation at which annual glacier accumulation and ablation are balanced. Since the ELA cannot be measured directly on the glacier, various methods have been established that can be used for the annual mass balance determination. The determination of the end-of-summer 'snowline altitude' (SLA) is used as an indicator for the ELA (Yuwei et al., 2014). The SLA of the past years can be used to parametrize and validate mass balance models. The mass balance of glaciers and its projection are used to indicate the implications of glacial changes for river runoff scenarios. The dependence of meltwater for drinking water, agriculture or water energy is considerable (Huss et al., 2017).

## 1.2 Glacier facies

Detecting the snow line on glaciers requires an accurate classification of various glacier surface facies. Creating a classification by fieldwork is very time-consuming which is why there was already interest in remotely sensed data in the mid-1970s. Various manual and automated classification approaches for supraglacial cover show that the resulting products meet a need in glaciology. Data about the snow line can be used to parameterize mass balance models. By implementing a longer

time series of snow line altitude data, mass balance models can be made more precise (Kääb et al., 2014; Paul et al., 2016; Rastner et al., 2019).

The meteorological conditions have a strong influence on the facies of a glacier. Weather changes also change the glacier surface. Snowfall in summer or rain in the ablation area can change facies types within hours (Williams et al., 1991). Besides the mentioned snow and glacier ice, there are also rock debris and glacial lakes that belong to the most frequent glacier facies (Rounce et al., 2017). Previous research has shown that the availability of cloud-free images is restrictive. This limitation calls for multisensor, pixel-based approach to better reconstruct interannual glacier changes. On a regional as well as on a global level, times series of the snow cover can be created. These snow cover statistics can be used for further analysis.

### 1.3 Research objectives

The aim of the thesis is to classify glacial surfaces over time and thus derive the snow line altitude evolution along with changes in glacial snow cover. This thesis investigates how a robust classifier can be developed, that can be applied in different glacial settings globally. Glacial settings can be defined for example by size, exposure or local climatic conditions.

Based on the glacier classification, we will validate different snow line altitude extraction approaches for glaciological applications. To exploit the current wealth of freely available satellite data (e.g. Sentinel-2 and Landsat), we will combine data from different sensors to increase the temporal resolution of long-term time-series analysis.

The entire processing chain is integrated in a fully automated program in the Google Earth Engine (GEE). The developed application can also be accessed via [www.slamonitoring.josiaszeller.ch](http://www.slamonitoring.josiaszeller.ch). This thesis explores the potential for glacier classification and analysis using the GEE framework, focusing on the following research questions.

RQ 1: How does the glacier facies classifier perform under different topographic settings?

RQ 2: With which accuracy can snow and ice on glaciers be distinguished from each other?

RQ 3: Which snow line altitude detection approach is best suited to extract the SLA?

### 1.4 Structure of the thesis

The remainder of this work is divided into six main chapters. Chapter 2 gives an overview of the target areas and the glaciological background. Chapter 3 then summarizes all optical satellite data, DEM and glacier outlines used in this thesis. This is followed by a description of the methods applied and developed in chapter 4. In chapter 5 and chapter 6 the results of this thesis and their discussion are presented. Finally, in chapter 7 we draw conclusions and outline potential ways in which our application can be used and developed in the future.

## 2 Target Areas and Glaciological Background

### 2.1 Target Areas

To develop, test and improve the classifier, several glaciers in the Ötztal Alps, Austria were chosen. This target area, covering approximately 500 km<sup>2</sup> in the south-west of Austria, serves to define thresholds for the classifier parametrization. The Ötztal Alps are highly suitable as study area, because three glaciers with mass balance measurements since 1952 are available. All three glaciers are used as reference glaciers for mass balance by the World Glacier Monitoring Service (WGMS). In addition to the mass balance data from the WGMS (2018), the area is also suitable because the glacier surface, and especially the snow cover, changes significantly due to precipitation, which occurs more frequently during the ablation phase from May to September. In the Ötztal Alps there is an accumulation of precipitation during the summer months (Pichler and Pasquini, 2009, Rastner et al., 2019). In the equilibrium line altitude (ELA) region, the mean annual temperature is -5°C and precipitation is about 1500 mm (Klug et al., 2018).

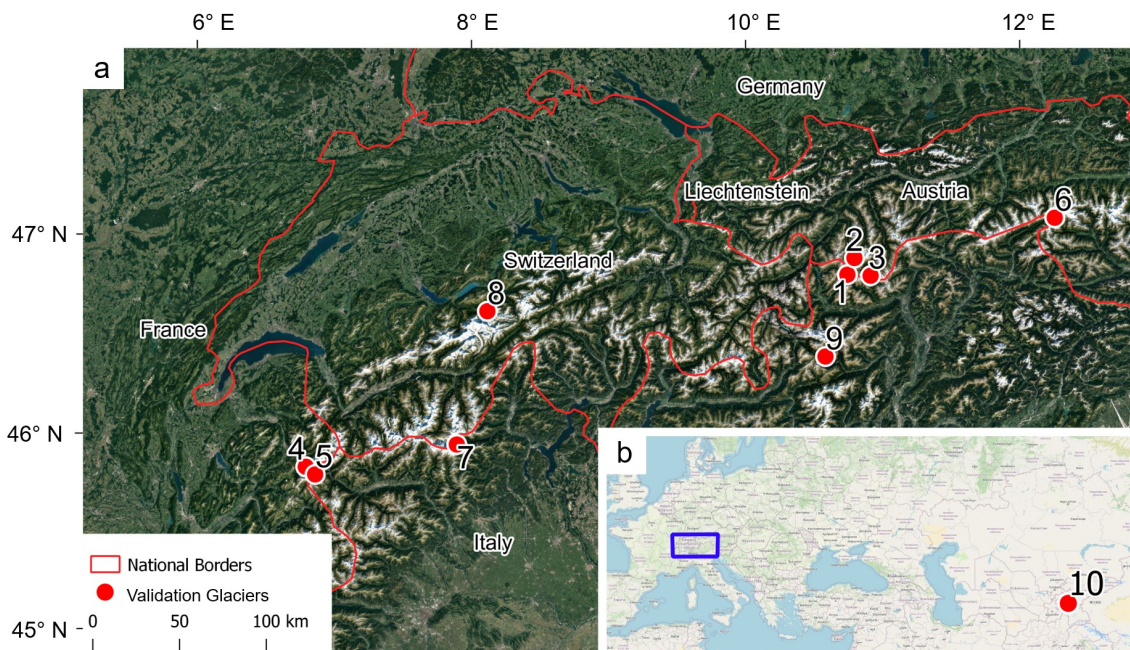


FIGURE 2.1: (a) Locations of the glaciers used in this thesis. Additionally to the 9 European glaciers, (b) the Abramov Glacier (10) in Kyrgyzstan is also used. The numbers of the glaciers refer to table 2.1, which also provides additional information on the size and exposure of the glaciers. Data basemap: a: Google Maps (n.d.), b: OpenStreetMap Contributors (2020)



TABLE 2.1: Overview of the glaciers used as target areas in this thesis. Global coordinates can be read from the GLIMS-ID, where ‘G’ is the prefix, followed by the east and north coordinates. The key indicators are derived from the Randolph Glacier Inventory (RGI) Version 6 and shows the state of the glacier at the time of the specified date.

#	GLIMS ID	Name	Country	Area [km <sup>2</sup> ]	min. Elev. [masl]	max. Elev. [masl]	mean Elev. [masl]	Slope [°]	Aspect [° AZM]	Source date	Annotation
1	G010758E46800N	Hintereisferner	AT	8.03	2430	3674	3051	16.2	71	Sept. 2003	WGMS Reference Glacier
2	G010818E46876N	Vernagtferner	AT	8.56	2810	3559	3142	14.70	165	Sept. 2003	WGMS Reference Glacier
3	G010791E46842N	Kesselwandferner	AT	3.96	2773	3460	3185	11.6	123	Sept. 2003	MB measurements since 1952/53
4	G006799E45819N	FR4N01239B04 du Miage 3	FR	0.62	2781	3612	3237	43.3	342	Aug. 2003	Small, Steep and Shady
5	G006846E45813N	Ghiacciaio del Miage	IT	10.99	1736	4776	2926	23.7	168	Sept. 2003	Large glacier with extensive debris cover
6	G012249E47078N	n.a.	AT	2.11	2292	3380	2751	30.6	342	Sept. 2003	Small, Steep and Shady
7	G007898E45942N	Ghiacciaio del Belvedere	IT	4.45	1797	4487	2833	27.3	42	Sept. 2003	Large glacier with extensive debris cover
8	G008119E46614N	Oberer Grindelwaldgletscher	CH	9.02	1361	3682	3026	24.1	281	Sept. 2003	Large, north-exposed glacier
9	G010590E46392N	Ghiacciaio dei Forni	IT	11.33	2484	3624	3144	19.5	348	Sept. 2003	Large, north-exposed glacier
10	G071570E39610N	Abramov	KGZ	21.34	3648	4895	4202	10	27	Sept. 2000	GTN-G Reference Glacier

Snow cover data from this region derived by an automated approach using Landsat data to determine the SLA, is used as reference data (Rastner et al., 2019). In order to validate the classification, we’ve included 6 other Alpine glaciers. Together with the Abramov Glacier in Kyrgyzstan, these 10 glaciers form the target areas. Table 2.1 lists all glaciers including the most important key indicators. Figure 2.1 shows the locations of the 9 European glaciers and the location of the Abramov glacier in Kyrgyzstan.

## 2.2 Glaciological background

This part discusses the glacier system in a way that the connections between remote sensing and glaciers presented in this thesis can be understood. Glaciers are formed where the snow accumulation is sufficiently large and the temperatures are low enough for the snow to remain in place during the summer. By increasing the density (evaporation, mechanical destruction, melting and refreezing) ice is gradually formed. When the ice mass becomes large enough due to the overlaying layers, the ice starts to flow down slopes due to gravity. At lower altitudes, a glacier loses mass through calving and melting (Cuffey and Paterson, 2010).

The equilibrium line altitude (ELA) separates the zone with mass gain (accumulation zone) from the zone with mass loss (ablation zone). The mass balance of a glacier is the direct result of the weather conditions and has thus a high correlation with the prevailing atmospheric conditions (Furbish and Andrews, 1984). This direct correlation between the mass balance and the atmospheric conditions shows that the surface cover can be used to assess the mass balance.

### **2.2.1 Measuring glacier mass balance**

The mass balance can be measured directly in the field with the glaciological method once or twice a year (Kaser et al., 2003). Such measurements are time-consuming and are only made for a few reference glaciers to continue a time series. A further measuring method is the geodetic method. This involves comparing the volume change at two points in time by calculating the volume difference between two terrain models. By comparing the two methods, the point measurements of the glaciological method can be calibrated (Cogley, 2009). However, due to the complex conditions of the two methods, a worldwide monitoring of the mass balance is not applicable.

Rabatel et al. (2005) show that it's possible to use snow line derived from satellite images as a proxy for the mass balance. With the use of satellite images and the automatic recognition of the snow line on satellite images it's possible to close data gaps.

### **2.2.2 Maximum SLA and ELA**

Rastner et al., 2019 show that the results of the classification of snow cover and the resulting SLA calculation show differences to the ELA. Despite the different ways in which the ELA is derived from field measurements, the agreement is promising. To compare the ELA with an SLA value, the maximum SLA during the ablation period must be determined. If no images of the end of the ablation period are available, the automatically mapped maximum SLA cannot be used as a proxy for the ELA or for the glacier mass balance.

Barandun et al. (2017) showed, that snow cover maps that do not show the maximum SLA aren't useless because they "[...] are an important input for albedo or degree-day factor parameterizations in mass balance models and have thus further applications" (Rastner et al., 2019). In addition to the ELA, the Accumulation Area Ratio (AAR) can also be used, which is directly related to the ELA. The AAR is the accumulation area in relation to the total glacier surface (Kaser et al., 2003).



### 3 Data

This chapter details, which datasets are used for the analysis. Using globally available data and implementing the entire process in the Google Earth Engine (GEE) makes it possible to study glaciers around the world. GEE is a cloud-based platform that provides access and the ability to process large geospatial datasets (Gorelick et al., 2017). An implemented algorithm in GEE can be used to analyse data and deploy an interactive application. GEE houses a multi-petabyte data catalog with publicly available datasets from satellite imaging systems. Additional datasets can also be easily added and combined with existing data.

In the first part, the optical datasets used are explained. This is followed by a section on the DEM and the glacier outlines used.

#### 3.1 Optical Data

We have chosen the optical data used in this thesis based on three main reasons (1-3) that are outlined in this section. The specific advantages of these datasets are then highlighted in the sub-chapters for the respective sensors. Glaciers and snow surfaces are subject to constant change. Due to the already mentioned dependence of glacier surfaces on the prevailing weather conditions, a high (1) *temporal resolution* is useful to detect these changes. To quantify changes in recent decades, a long time series of satellite images also contributes to the prolongation in temporal resolution. Figure 3.1 illustrates the development of image availability over the last 40 years. Based

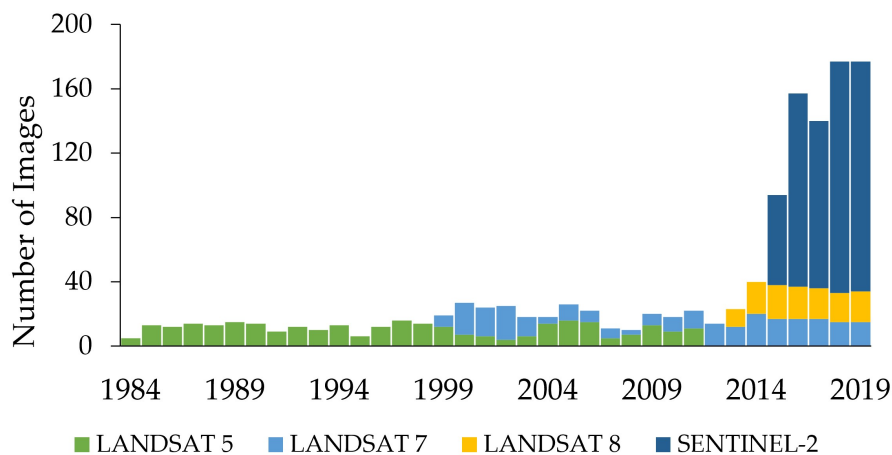


FIGURE 3.1: Image availability of Landsat 5, 7, 8 and Sentinel-2 for the target Area in the Ötztal Alps, AT from 1984 to 2019. The figure highlights the pronounced increase in image availability since the launch of the Sentinel-2 satellites.

TABLE 3.1: Spectral bands of Landsat 5, 7 and 8 and Sentinel-2A and 2B used in this thesis.

	Landsat				Sentinel		
	Wavelength (nm)			Res. (m)	Wavelength (nm)		Res. (m)
	Landsat 5	Landsat 7	Landsat 8	<i>*resampled</i>	Sentinel-2A	Sentinel-2B	<i>resampled</i>
Blue	450-520	450-520	450-510	30	448-546	443-541	20
Green	520-600	520-600	530-590	30	538-583	536-582	20
Red	630-690	630-690	640-670	30	646-684	646-685	20
NIR	760-900	770-900	850-880	30	763-908	767-900	20
SWIR 1	1550-1750	1570-1650	1566-1651	30	1542-1685	1540-1681	20
SWIR 2	2080-2350	2100-2290	2107-2294	30	2081-2323	2067-2305	20
TIR 1	1040-1250	1040-1250	1060-1119	30*			
TIR 2		1150-1251		30*			

on (2) *multispectral satellite data* it is possible to study glacier surfaces. The spectral differences of snow and ice are represented in the visual (VIS), near-infrared (NIR) and shortwave infrared regions (SWIR) of the spectrum. Due to the fine differences between the spectral properties (c.f. Käab et al., 2014, Rastner et al., 2019), a high spectral resolution is essential for the challenging classification. Glacier surfaces have small-scale structures that can only be visualized with a high (3) *spatial resolution*. This point is crucial, because there are many small-scale glaciers ( $>2.5 \text{ km}^2$ ) in addition to the large and partly known glaciers. For an accurate snow line altitude (SLA) and snow covered are (SCA) determination a high spatial resolution is necessary. In this thesis we use images with 30 m (Landsat) and 20 m (Sentinel-2) resolution (see table 3.1). With these spatial resolution values, there is a balance between a realistic classification and the computing time required. The suitability of images for our analyses is influenced by seasonal variations. Various filters are implemented in the program to deal with these conditions. Sentinel-2 data have been available since mid-2015. Due to the increased availability of images, the temporal resolution of the study period is improved. We use calibrated top-of-atmosphere (TOA) reflectance data (see Chander et al. (2009) for Landsat data and ESA (2015) for Sentinel-2 data), where the surface and atmospheric reflectance is combined. By omitting an atmospheric correction the between-scene variability is reduced.

### 3.1.1 Landsat 5, 7 and 8

Landsat images are available since 1984 until today and have a spatial resolution of 30 meters. Consequently, the Landsat program provides the longest time series of high-resolution multispectral satellite imagery. All sensors cover the range of visual, NIR and SWIR wavelengths. For Landsat 7 and 8, two additional thermal bands are available. Table 3.1 shows the bands per sensor that are used in this thesis. The Landsat time series has a temporal resolution of 16 days at the equator. Landsat 7 data has a limited spatial coverage since a failure of the Scan Line Corrector (SLC) in May 2003, resulting in a repeated wedge-shaped pattern along the image edges (Chander et al., 2009). These data gaps can have an impact on the extraction of the SLA and snow cover. Due to the data gaps, SLA extraction may not work if the area of the SLA is affected by the gaps. If the data gaps affect large parts of the glacier, this can also have a major impact on the SCR, as

TABLE 3.2: Comparison of three freely available DEM. In this thesis the ALOS-DEM is used, because it has a higher accuracy and potentially a higher spatial resolution compared to SRTM and ASTER (ALOS: Takaku et al., 2014, SRTM: Farr et al., 2007, ASTER: Tachikawa et al., 2011).

Name	Imaging System	Spatial Resolution	Horizontal Accuracy	Vertical Accuracy	Year	GEE-Availability
ALOS	Optical	30 m, commercially: 5 m	5 m	5 m	2006 - 2011	Yes
SRTM	SAR C band	30 m	<20 m	<16 m	2000	Yes
ASTER	Optical	30 m	30 m	20 m	2008 - 2011	No

potentially snow-covered or snow-free areas must be omitted completely. Landsat 5 and 7 have a lower radiometric resolution resulting frequently in saturated visual bands over snow and cloud-covered areas. Images with over-saturated pixel values are marked and could be filtered. By using bands outside the VIS bands, over-saturated pixels can also be classified.

### 3.1.2 Sentinel-2

Sentinel-2 is a high-resolution, multi-spectral mission. By using twin satellites flying in the same orbit, a temporal resolution of 5 days at the equator is possible. The spatial resolution in the VIS and NIR range is 10 m and SWIR 20 m (ESA, 2015). The higher temporal resolution enables denser time series, which means that non-usable, cloudy scenes have less impact on data availability. With the improved spatial resolution, small-scale variations such as moraines or supraglacial lakes on the glacier surfaces can be considered. The wavelength differences between the two sensors (see table 3.1) are very small with Sentinel-2 and are therefore neglected. In our analysis, we resampled the spatial resolution of the VIS bands to 20 m.

## 3.2 Digital Elevation Model (DEM)

The choice of the DEM was determined by the global data availability. Besides the extraction of a snowline altitude, the calculation of the shadow cast by the topography surrounding the glacier (hillshadow) is based on the DEM itself.

The availability of freely available global DEM is limited. The ALOS DEM (Advanced Land Observing Satellite by Japan Aerospace Exploration Agency, JAXA) has a resolution of approximately 30 m and was generated from a stereo mapping sensor operated from 2006 to 2011. The DEM with a 5-meter resolution resulting from this mission forms the basis for the freely available 30-meter resolution DEM (JAXA, 2017). The accuracy of the ALOS-DEM is at an RMSE of 5 m vertically (Prioretti et al., 2017).

Table 3.2 compares the ALOS-DEM with SRTM and the ASTER. Due to the higher accuracy and the possibility to increase the spatial resolution, this thesis uses the ALOS-DEM.

### **3.3 Glacier outlines**

The Randolph Glacier Inventory (RGI) is a dataset that provides outlines of approximately 200'000 glaciers worldwide. When creating the dataset, completeness was the primary goal. The outlines represent the glaciers at different times and are not updated annually (Pfeffer et al., 2014). Table 2.1 lists all RGI shapefiles used in this thesis. In addition to the date of creation, further key indicators, additional information on the glaciers and annotation regarding their use in this thesis are included.

### **3.4 ELA and AAR Data by the WGMS**

The equilibrium line altitude (ELA) values indicate the altitude, where net mass change is zero. This altitude is calculated using the specific mass balance for each individual altitude interval. With a vertical mass balance profile (VBP) the ELA can now be derived. The AAR values are determined from the calculated ELA and show the ratio between accumulation and ablation at the end of the balance year (Kaser et al., 2003). The ELA and AAR values used for the validation are provided by the WGMS (2018) and were collected for the Vernagtferner by Christoph Meyer et al. (Bavarian Academy for Sciences, Munich, DE) and for the Kesselwandferner by Irmgard Juen et al. (University of Innsbruck, AT).

## 4 Methods

In this chapter the process of data preparation, classification and extraction of the snow line altitude (SLA) is outlined. Figure 4.1 shows in simplified form how the entire process is implemented in the GEE framework. The process is started with a GUI and ends fully automatically with the export of data from a glacier from the selected period. After startup by the user, the selected and filtered images are classified in the GEE and can be exported as GeoTiff for control purposes or for an alternative type of analysis outside the GEE. The analyzed data of the snowcover and the snow line altitude for the selected glacier withing the time period can be exported as CSV file (comma-separated values).

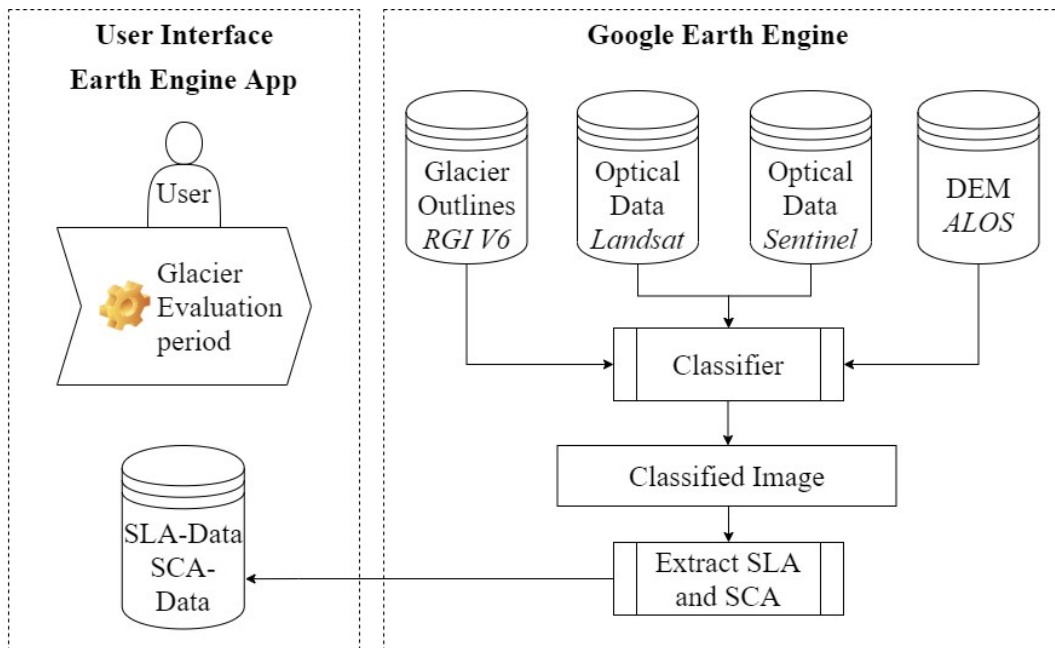


FIGURE 4.1: Simplified architecture of the process of analysing the snow line altitude (SLA) and the snow covered area (SCA) of glaciers within the Earth Engine-Framework

The structure of the chapter follows the structure of the program and assigns the subchapters to individual steps and modules of the developed program. Figure 4.2 illustrates how the program is structured and which individual modules are called. The modular structure makes it possible to adapt individual steps or to extend them with additional modules.



The code of the modules and the application can be found at [www.slamonitoring.josiaszeller.ch](http://www.slamonitoring.josiaszeller.ch).

In the first part, the filtering and data preparation is shown. This is followed by a description of the classification methods, and finally three approaches are presented for extracting SLA values from the classified data. Figure 4.2 also shows the simplified structure of the modular program, whose process runs from top to bottom. The fully automated program starts with a user input that defines a glacier and an evaluation period.

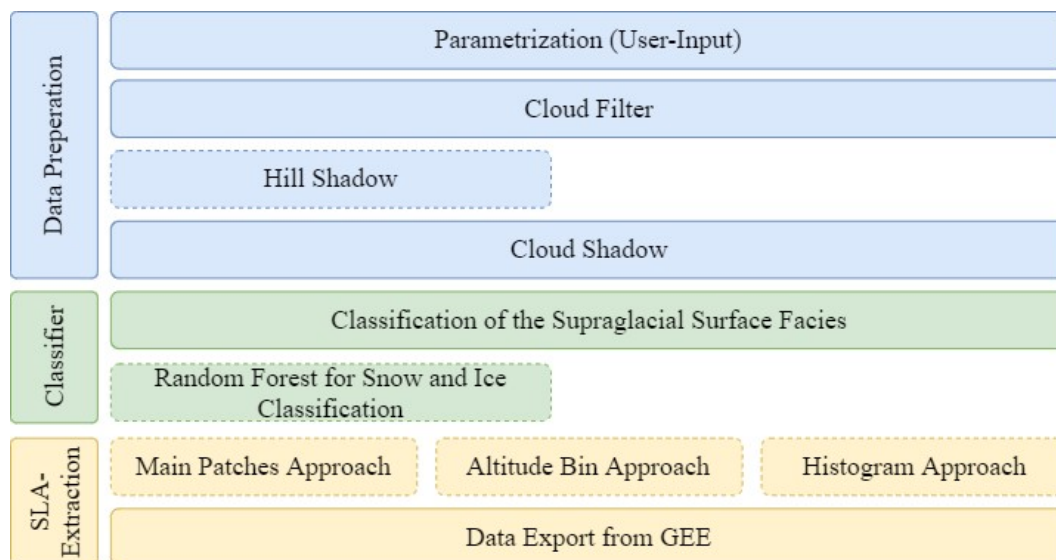


FIGURE 4.2: General overview of the structure of the modules that are called up from top to bottom. Blue are modules for data preparation and filtering. Green indicates the classification of the prepared images and yellow shows three modules for SLA extraction. Dotted lines around the modules mark the optional modules, which can be selected by the user.

## 4.1 Preparation of Data

Using the information of the user input, an image collection is created from the available images. In this collection, the images of all sensors (Landsat 5, 7 and 8 as well as Sentinel-2) are sorted by time of acquisition. In this first step the images are also checked for duplicates and the bands and scaling of the different sensors are harmonised.

### 4.1.1 Add Albedo Band

In addition to the available bands, which differ in the sensors, an additional band with the albedo according to Liang et al. (2003) is added. In this thesis, the albedo is used for a Random Forest classifier, which is used to create training datasets with information from additional bands (see chapter 4.3). Naegeli et al. (2017; 2019) use Albedo products to assess glacier surfaces and extract mass balance proxies from them.

$$Albedo = 0.356 * Blue + 0.130 * Red + 0.373 * NIR + 0.085 * SWIR1 + 0.072 * SWIR2 - 0.0018$$

### 4.1.2 Cloud filter

For each image in the collection a cloud-score is calculated, which indicates the cloud-free area within the glacier outlines. It's important not to use the cloud score from the image metadata, but that an individual score is calculated for each glacier. The cloud cover in the mountains is strongly dependent on the topography. Due to the partly small-scale glacier areas in the high mountains, it's possible that they are cloud-free, despite a high cloud coverage over the whole image. This allows the image collection to be individually filtered with a user-selectable threshold. The cloud filter creates a cloud mask for each image, which is used to calculate the cloud covered area for each glacier. The high reflectivity in the visual and infrared range of the spectrum (NIR and SWIR) is used for cloud detection. The cloud score algorithm is adapted to work with all sensors and uses the same bands (Red, Green, Blue, NIR, SWIR1 and SWIR2). With every iteration of the program, a new mask is calculated for each image, which also makes it easy to apply threshold changes or scaling adjustments. To distinguish snow from clouds, the Normalized Difference Snow Index (NDSI according to Hall and Riggs (2010)) is taken into account. Depending on the region, a high cloud cover threshold can result in extended data gaps in the image time series. For the year 2019, with a threshold of 70 % cloud-free images of the Hintereisferner, there is a median temporal difference of 3.5 days between two subsequent images. However, between the end of July and the end of August there is a gap of 32 days. For Kesselwandferner, the glacier next to it, this gap is only 15 days between July and August and for Vernagtferner the gap is 26 days. If these data holes occur coincidentally at the end of the ablation phase, this can lead to greater deviations between the automatically determined SLA and the ELA data from the WGMS.

## 4.2 Classification

The aim of the classification of glacier surfaces is to extract information in a standardised way using the classified images. The pixelwise classification is explained step by step in this chapter. Figure 4.3 illustrates the decision tree that is processed for each pixel on the image. Each pixel is assigned to one of the seven classes. These classes can then be used for the subsequent extraction of data without having to consider satellite images with multiple bands. The decision tree is an elimination process, in which a pixel of the image is masked as soon as it fits one of the predefined classes.

### 4.2.1 Classes

The images are classified into seven classes that are listed in table 4.1. The classes represent only the glacier surfaces. Water on the glacier surface is classified as water or a debris cover glacier tongue as debris cover. The classification can therefore not be directly used to map a glacier outline or the length changes of glaciers.

Classes 0 to 4 form the main classes. Class 6 indicates shadows on snow. Class 8 combines the different types of shadows. The intentionally omitted numbers could be used to assign a corresponding shadow class to each main class.

In the classification method presented here, only shadow on snow (class 6) is kept separately. The

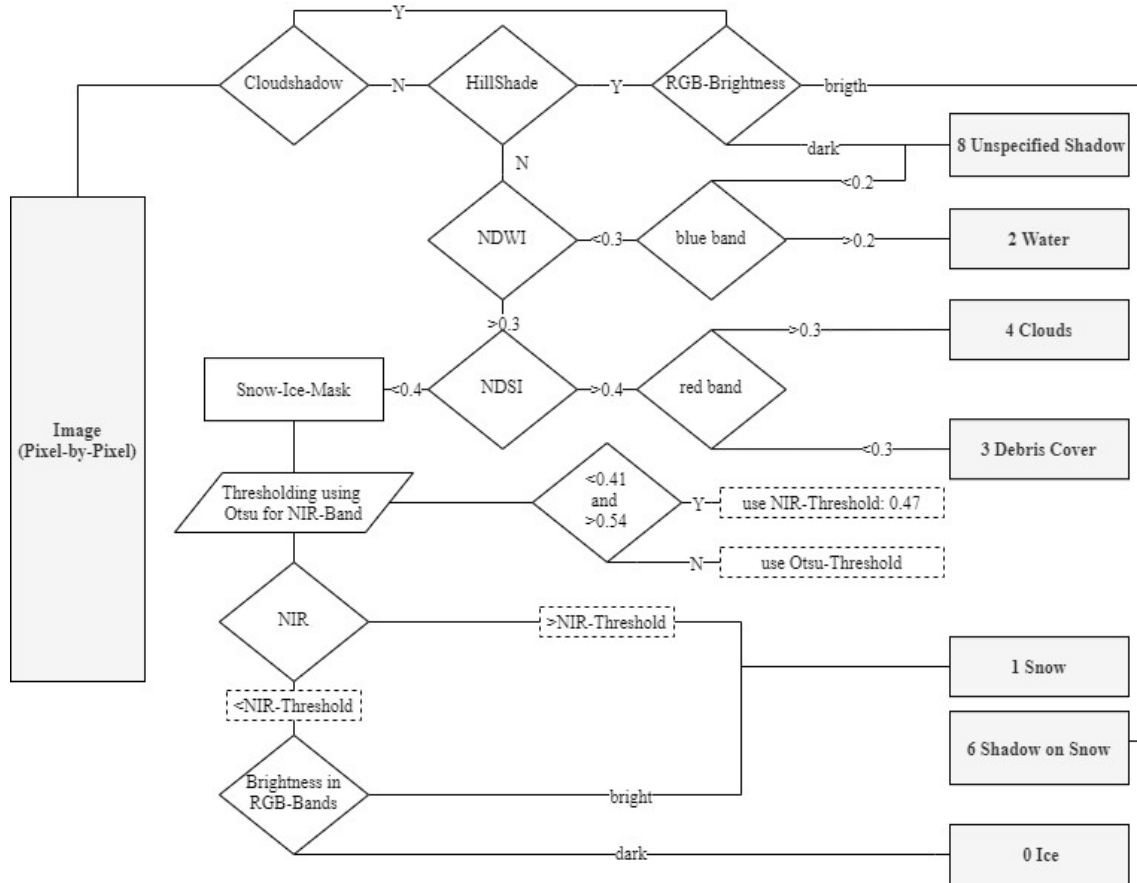


FIGURE 4.3: Workflow for the pixelwise allocation in one of the classes (c.f. Table 4.1). Each pixel is assigned to a class independently by this process. Fixed and automatic threshold values are used for the classification.

division of shadows on different glacier facies would be interesting in so far as the use of the classification method would also be possible in heavily shadowed areas (e.g. in steep valleys with a lot of topographic shadow).

#### 4.2.2 Hill Shadow

The pronounced topography, in which many glaciers form, means that, depending on exposure, there is a lot of shadow in the area to be classified. To calculate the shadow cast on the glacier surface, the ALOS-DEM and the solar position (azimuth and zenith) are used to determine the illuminated and shadowed areas on the glacier. The hill shadow calculation is limited to an area of 2500 m around the RGI-Outline.

TABLE 4.1: The table shows the classes applied by the classifier with the corresponding numbers. The classes correspond to the attributes when exporting classified images at the end of the process.

Number	Class
0	Ice
1	Snow
2	Water
3	Debris Cover
4	Clouds
6	Shadow on Snow
8	Unspecified Shadow

### 4.2.3 Cloud Shadow

Clouds can cast shadows on glaciers. Small clouds, which are close to the glacier surface and whose proportion is below the filtered maximum cloud cover, cast small-scale shadows on the surface. The detection of cloud shadows on glaciers can prevent misclassifications, since the spectral signals of shadowed snow can be similar to those of ice.

To detect cloud shadows on the glacier surface, clouds are detected on the glacier and within a 2500 m buffer zone around the glacier outline. The detected clouds are then projected onto the surface based on the position of the sun. This method was introduced by Martinuzzi et al. (2007) and programmed in a simple version by Donchyts (2016). During this cloud shift the clouds are modelled in 25 m steps up to a projection height of 500 m above the ground. Clouds are only recognized in a radius of 2500 m around the glacier, because the image is cut with this boundary. This reduces the amount of data to be handled, which speeds up the process. If this projection intersects a pixel that appears dark in the NIR, SWIR1 and SWIR2 bands, this pixel is marked as a shadow (class 8).

### 4.2.4 NDWI and NDSI

After the hill shadow and cloud shadow processing, the non-shadowed area remains. Water and shadows are extracted from this area using the Normalized Difference Water Index (NDWI: Huggel et al., 2002) with a threshold of 0.3. The potential shadow can come from unrecognized clouds or from small topographical elements such as boulders or deep crevasses that are not included in the DEM. The distinction between water and shadow is made with a fixed threshold on the *blue* band of 0.2.

The Normalized Difference Snow Index (NDSI: Hall and Riggs, 2010) is used to separate between snow or ice from clouds and debris cover. A threshold of 0.4 is used for the NDSI. The *red* band divides the area remaining (clouds and debris cover) by a fixed threshold of 0.3 into the classes clouds and debris cover.

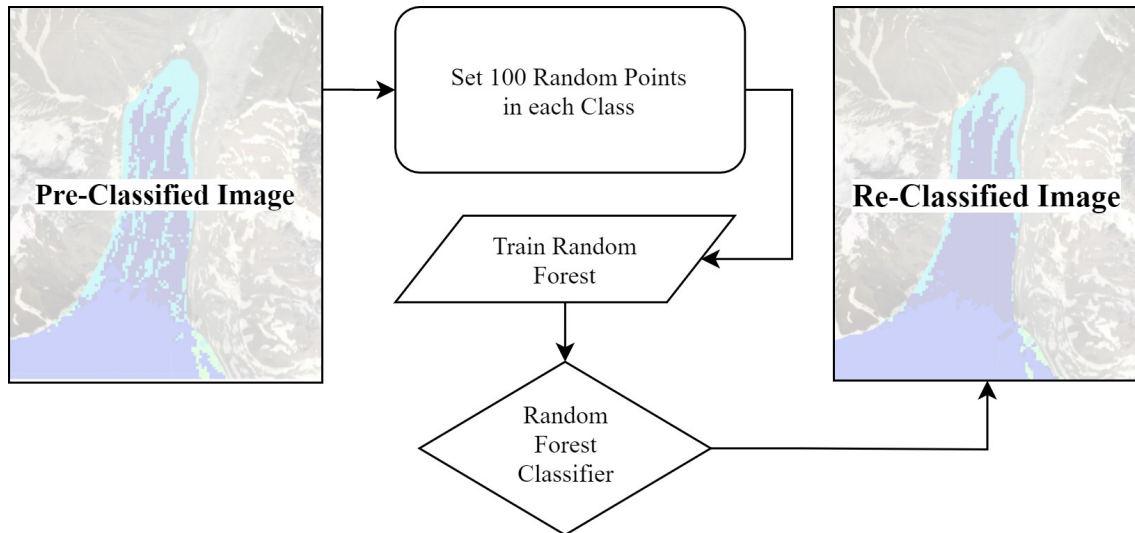


FIGURE 4.4: Workflow of the self-training Random Forest classifier in the GEE-Framework. The pre-classified image is the result of our Decision Tree classifier. In each class of the pre-classified image, 100 random points are set to create a training dataset for the Random Forest classifier.

#### 4.2.5 Otsu with NIR

The remaining area may contain snow, ice or both. In order to divide this area, the Otsu-threshold method (c.f. Otsu, 1979) is used to set a threshold for the *NIR* band. The limit is set assuming that there are two classes in the remaining area. A bimodal histogram is used to maximize the between-sum-of-squares (BSS) and thus set a threshold for the *NIR*-band. Since the condition that there are two classes (snow and ice) in the image is not always fulfilled, the Otsu threshold is only used if it falls within a certain interval ( $<0.41$  and  $>0.54$ ). If the Otsu-threshold is outside this interval, a fixed value of 0.47 is used.

With this threshold the remaining area can be divided into the two classes snow and ice. Pixels that lie above the *NIR* threshold but appear very bright in the RGB bands are assigned to the snow class with a final reclassification.

### 4.3 Random Forest

Random Forest (RF) is a machine learning approach that can be used as a classifier for satellite images. RF already works with a small training dataset, but can also process many training points quickly (c.f. Breiman, 2001, Waske et al., 2012). The lack of a globally usable training dataset for the distinction between snow and ice cover on glaciers led to the idea to train the RF-Classifier directly with the image to be classified. With the illustrated Decision Tree (see chapter 4.2) the glacier surface is divided into seven classes. These classes are now used again to train the classifier and re-classify the glacier surface. In all classes, 100 points are set at random, which are then used as a training dataset. For the classification with the Random Forest classifier the bands are used that are available with all sensors (*red, green, blue, NIR, SWIR1, SWIR2*). The Albedo according to Liang et al. (2003) is also used as an additional band. Figure 4.4 shows the process of the classifier, which can be seen as an extension to the classifier presented here.

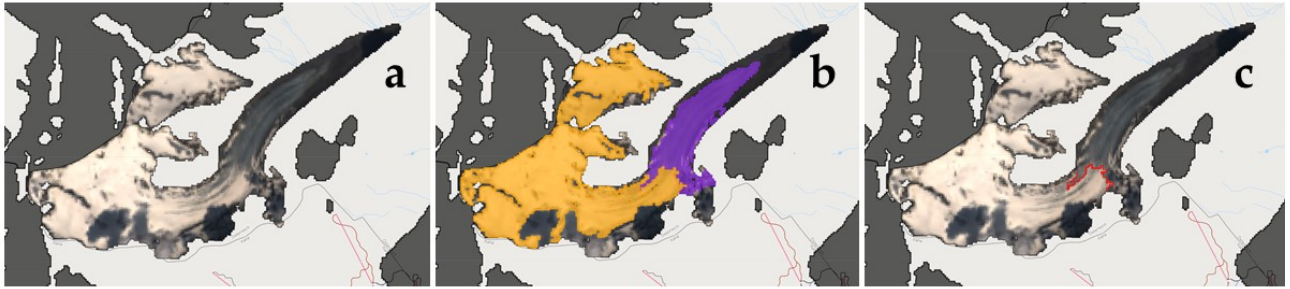


FIGURE 4.5: Example for determining the SLA with the Main Patches Approach. 4.5a shows the original image within the RGI-Outlines. 4.5b shows in orange the snow patch and in purple the ice patch. Image 4.5c shows a red line, where the snow- and icepatch met. The SLA is the median of the altitude values of the pixels on this line.

*Landsat 8 - Hintereisferner (AT), 27th July 2019*

## 4.4 SLA and SCR Extraction

After classifying the images into the seven classes, the next step is to extract information about the SLA and the SCR from the images (see figure 4.1). For this extraction, three methods (Main Patches approach, Histogram approach and Altitude Bin approach) are implemented in the program, which work independently of each other.

### 4.4.1 Main Patches Approach

The Main Patches approach uses only the area classified as ice and snow. All other areas are masked out and are dropped. Following this, the largest patches of both classes are determined (see figure 4.5b). The snow line is where the two main patches of snow and ice meet. The median altitude of the pixels marking this snow line is determined and extracted as the SLA.

In addition to the SLA, the standard deviation of the altitude values used for the SLA determination is given. The higher this number, the less representative the SLA value given is for the snowline height on the glacier. It should be noted that the standard deviation also depends on the length of the detected snowline. The smaller the area where the patches touch, the smaller the standard deviation will be.

To extract an SLA value for all scenes, additional rules have been established. Table 4.2 shows the hierarchy of the rules. With these rules, an SLA can be extracted for all classified images. It should be noted that the first and last rules are less precise approximations than the second rule. The additional information provided by the Main Patches approach can be used to specify the rule used to determine the SLA.

TABLE 4.2: Main Patch Approach: Hierarchy of rules applied for SLA extraction

Hierarchy	Situation	Resulting SLA-Value [m.a.s.l.]
1	<95 % snow cover on the glacier surface	Lowest elevation of the RGI Glacier Outline
2	Ice- and Snowpatch touch each other	Median of the elevation values of intersection line
3	Patches do not touch each other	Lowest elevation of the biggest snow patch

#### 4.4.2 Histogram Approach

The Histogram approach is based on the different area distribution per altitude of the two main classes snow and ice. With both classes, a histogram is created based on the altitude values. The two histograms are then used to find the smallest area difference at an altitude level (c.f. figure 4.6. To define the SLA, both histograms are used to find the altitude level where the area difference between snow and ice is minimized and the area sum is maximized. The altitude levels are defined by the number of bins in the histogram. The Histogram approach is based on an idealized snow distribution on the glacier, where snow covers the whole area from a certain altitude. Due to the occurrence of smaller snow-free ice patches in areas above the SLA, there is a rule hierarchy in the extraction that is adhered to. These rules, which are listed in table 4.3, cover all situations that may occur in the images to be processed. This ensures that the approach does not cause the processing of a time series to interrupt.

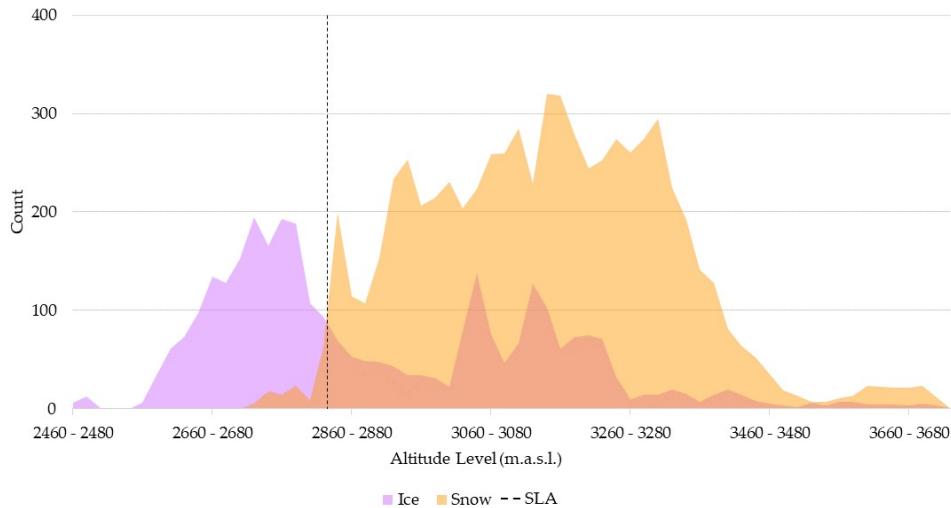


FIGURE 4.6: Histogram with the area distribution per altitude level of snow in orange and ice in purple. The dotted line shows the approximated SLA where the area distribution differences are minimized and at the same time the area sum is maximized. To put it in a nutshell, the SLA is where the two histograms intersect.

*Histogram based on a Landsat 8 image from Hintereisferner (AT), 27th July 2019*

TABLE 4.3: Histogram Approach: Hierarchy of rules applied for SLA extraction

Hierarchy	Situation	Resulting SLA-Value [m.a.s.l.]
1	>90 % snow on the glacier	Lowest elevation of the RGI glacier outline
2	Snow and ice on the glacier	Altitude, where the area difference is minimized and the area sum is maximized
3	0 % snow on the glacier	Highest elevation of the RGI glacier outline

### 4.4.3 Altitude Bin Approach

The Altitude Bin approach is based on the SLA extraction of ASMAG (see Rastner et al., 2019). In the implemented variant, however, the approach is divided into two parts. In the first part the snow and ice ratio is approximated for all altitude bins. In the second step the SLA and SCR are extracted from these altitude bins.

For the approximation of the snow cover, the classified image is divided into two categories (snow and ice). For each bin, the surface which is not classified as ice or snow (see table 4.1) is allocated to the two categories in the same proportion as ice and snow in the corresponding altitude bin. For example: the altitude bin from 3000 m to 3050 m is covered with 30 % snow, 40 % ice and 30 % cloud cover. The 30 % cloud cover is now divided in a 3:4 ratio. This results in a distribution into the two categories of 42.86 % snow and 47.14 % ice. If there is no snow or ice in an altitude band, this altitude band is not included in the approximation.

Figure 4.7 shows an example of the area distribution per altitude level. The figure displays

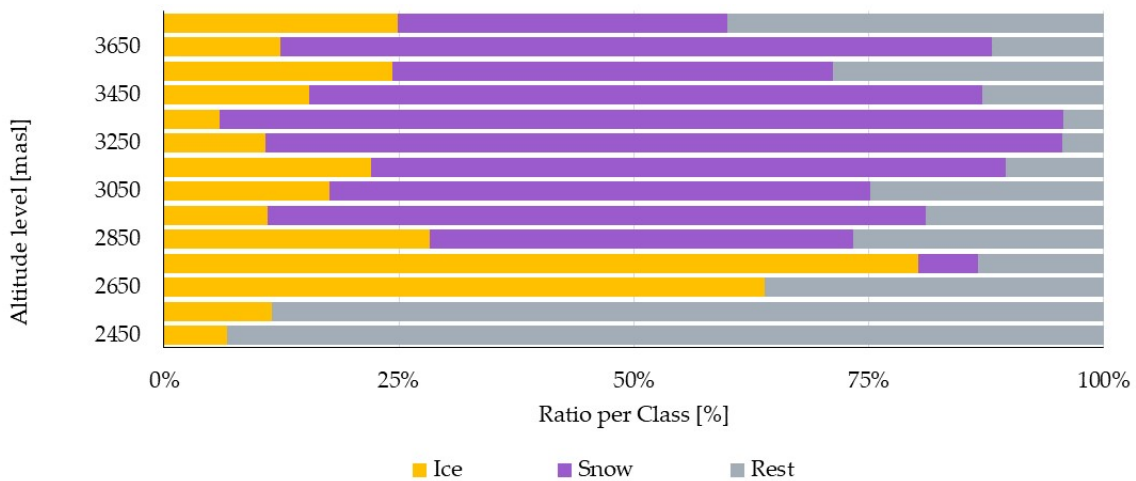


FIGURE 4.7: Example of the area distribution per height level for the Hintereisferner at the end of the ablation phase 2019. The grey part (rest) combines the classes Debris Cover, Clouds, Water and Shadow. In a next step, this area will be proportionally allocated to the classes Snow and Ice.

values of the Hintereisferner from an image at the end of summer, where ice occurs at the highest altitudes. The glacier surface is divided into altitude bins of 50 m. In these bins the described approximation is made into the two categories snow and ice. The sum of the categories snow and ice is then 100 % for all bins. From the lowest bin the program searches three adjacent bins are at least 50 % snow covered. If this is the case, the lower limit of the first bin of the triplet is output as SLA. Table 4.4 shows the hierarchy of the rules applied to determine the SLA.

TABLE 4.4: Altitude Bin approach: Hierarchy of rules applied for SLA extraction

Hierarchy	Situation	Resulting SLA-Value [m.a.s.l.]
1	No Altitude Bin with snow cover (SC) >50 %	Lowest altitude of the RGI glacier outline
2	No group of three bins where SC >50 %	Lower boundary of the first bin, where SC > 50 %
3	3 adjacent bins with >50 % SC	Lower boundary of the first bin of the group



## 4.5 Implementation as a GEE App

To be able to use our program, we have developed a simple Google Earth Engine GUI. This allows a user to select any glacier from the Randolph Glacier Inventory and define an investigation period. In addition, values for the cloud cover filter and the hill shadow mask can be parameterized. If Landsat or Sentinel-2 images are available for the selected time period, they are classified fully automatically and the SLA and SCR data are extracted using the Main Patches approach and the Altitude Bin approach. This data is then computed in the background and stored directly in a personal cloud storage. Figure 4.8 shows a screenshot of the GEE application, which can be accessed on [www.slamonitoring.josiaszeller.ch](http://www.slamonitoring.josiaszeller.ch).

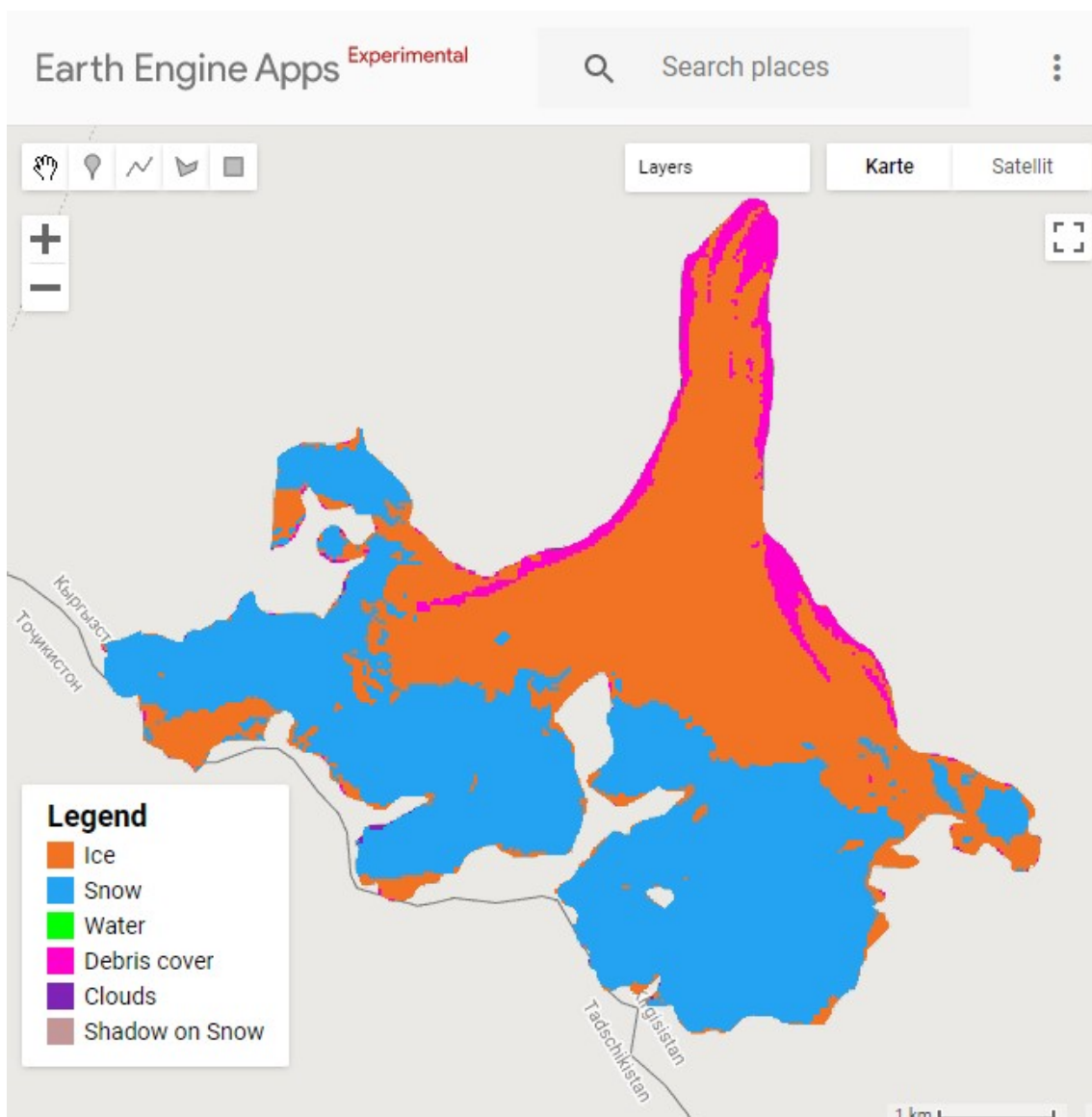


FIGURE 4.8: Screenshot of the Earth Engine App developed by us. The classified map shows the Abramov glacier and is based on a Landsat 5 image from August 22, 2011. The app can be accessed via [www.slamonitoring.josiaszeller.ch](http://www.slamonitoring.josiaszeller.ch). The scene belongs to one of the 44 scenes classified for the validation of the SLA extraction method (see chapter 5).

TABLE 4.5: Metadata about the values included in the export

Attribute	Unit/Type	Approach	Notes
		MP = Main Patches Approach Histo = Histogram Approach AB = Altitude Bin Approach	
<b>system:index</b>	Text	MP, Histo, AB	Name of the scene origin: Sensor info (Landsat 5, 7 or 8, Sentinel-2) and date
<b>date_MSxlsx</b>	Days since 1.1.1900	MP, Histo, AB	Date in Microsoft data format (1900-date-system)
<b>otsu</b>	0-1	MP, Histo, AB	Value of Otsu analysis (histogram on NIR-Band) on the snow/ice surface
<b>SLA</b>	m.a.s.l.	MP, Histo, AB	Snow Line Altitude, based on the ALOS-DEM
<b>system time_start</b>	Sec since 1.1.1970	MP, Histo, AB	Unix timestamp with three decimal places, Time of image acquisition
<b>Snow Cover Ratio</b>	%	MP, AB	Area classified as snow in proportion to the total area of the RGI-Outline
<b>Ratio Area w/o Snow and Ice</b>	%	MP, AB	Proportion of non-snow and non-ice (clouds, water, debris cover, shadow)
<b>Area for MP-SLA-Extraction</b>	%	MP	Proportion of the area of the main patch ice and snow
<b>Std Dev MP</b>	meter	MP	Standard Deviation of the Snow Line Altitude

For each method, the images to be analyzed are evaluated individually and the data are summarized in a CSV file. Depending on the method, the exports are available with different attributes. In addition to the SLA (Snow Line Altitude in m.a.s.l.) and the SCR (Snow Cover Ratio as percentage of the total area of the glacier), additional values are given which, if desired, can be used to weight the data in modelling. All attributes of the exports are listed in table 4.5 , which also shows the units of measurement of the values.



## 5 Results

This chapter is divided into three sub-chapters, each of which is focussing on one aspect of the program. The first part evaluates the classification, which is used as a basis for further processes. In the second sub-chapter the extraction of the SLA and the SCR is examined. The three methods (c.f. chapter 4) are compared and validated with independent datasets. In the last part, the use of time series made possible by the increased availability of satellite images is analysed.

### 5.1 Validation of the classification

Due to missing data for a direct validation of the classification, this sub-chapter is divided into two parts. In the first part, the classified snow surface is qualitatively compared with data from Rastner et al., 2019. The second part compares and quantifies the classification based on 6 manually digitized snow cover maps from independently selected glaciers in the Alps.

#### 5.1.1 Qualitative comparison with ASMAG (Rastner et al., 2019)

The automated tool 'ASMAG' (automated snow mapping on glaciers) can be used to map snow cover and derive the SLA. ASMAG uses Landsat images and includes an internal pre-processing of the images. An Otsu threshold is determined for each image with the NIR band. With this threshold, the image is then classified into two classes (snow and non-snow). The glacier outlines used by ASMAG are manually updated lines that represent the outlines of the glacier at the end of august 2011 (Rastner et al., 2019).

The qualitative comparison of the snow cover maps serves to show differences in the classification of the same images. Four scenes from the Hintereisferner (see table 2.1) between 1990 and 2011 were selected. Figure 5.2 and 5.1 show the snow cover by Rastner et al. (2019) which is unmodified and overlays pixels classified as snow in green. The snow surface classified by our classifier of this thesis is shown in purple. All other remaining classes are hidden. It should be noted that the two classifications are not based on the same outlines. The map created in the context of this work is based on RGI-Outlines Version 6, which are quite different to the outlines used by ASMAG. In the case of the Hintereisferner a part of the glacier in the northwest was not used, which according to the RGI also belongs to the glacier area.

A comparison between the two classified images is shown in figure 5.1 and 5.2. Figure 5.1 shows two scenes where the classified snow cover is well comparable. Figure 5.2a shows an image, where

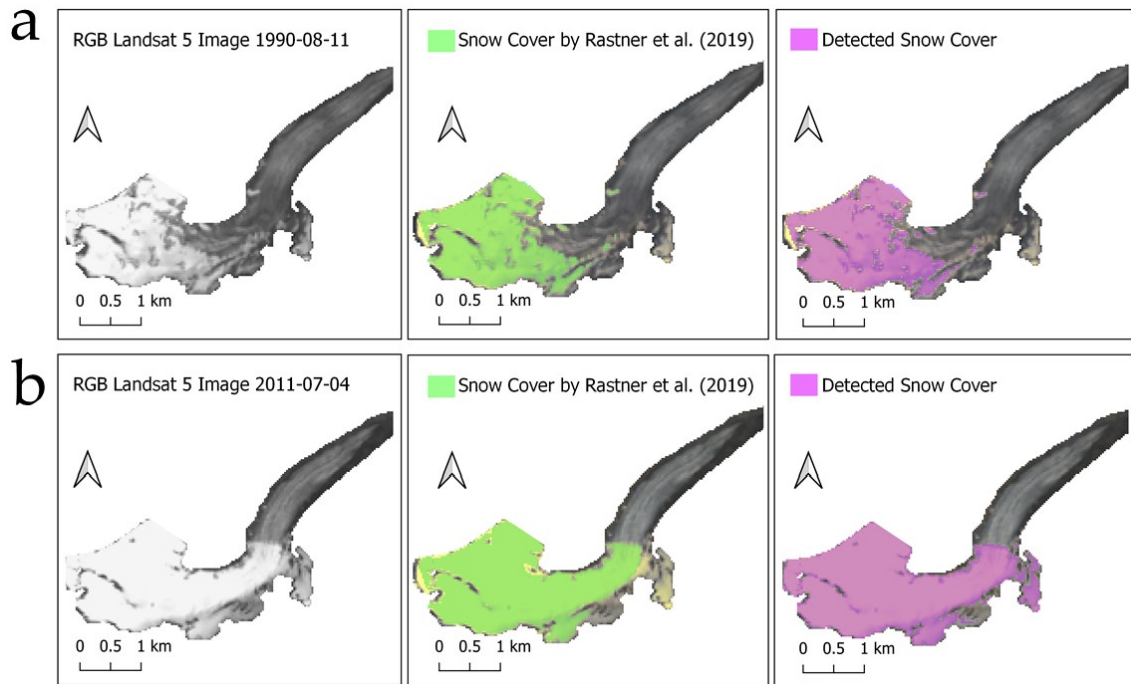


FIGURE 5.1: This figure shows the snow cover map by Rastner et al. (2019) in green and in purple the achieved result of the presented classifier from 1990 (5.1b) and 2011 (5.1b). In both triplets, only very small differences in classification can be seen on this scene. The used Otsu-Thresholds are calculated on the NIR band for all, but the area used for the threshold determination is not the same.

In triplet 5.1a a difference can be seen in the area of the small bulge in the northeast. This is due to the fact that the two methods do not use the same glacier outlines.

clouds are classified as snow in the classification of Rastner et al. (2019). In our method clouds are classified as clouds. The image from 2007 (figure 5.2b) shows a clear difference in the snow classification. Our classification method classifies a much larger area as snow than the snow cover map from Rastner et al., 2019. Our classifier re-analyses the area already classified as ice with the Otsu threshold and the NIR band and looks at the brightness in the visual spectrum (*red*, *green* and *blue*). If the pixels classified as ice in these bands are bright enough, they are reassigned to the snow class.

### 5.1.2 Validation with visually drawn snow cover classifications

In a subsequent step the classification of snow is validated outside the target area. For this, 6 different Alpine glaciers were selected. The 6 glaciers are number 4 to 9 from table 2.1, where the glaciers are described with the key indicators. For these 6 glaciers, selected independently of the target area, an attempt was made to cover a wide range of glacial characteristics. The glaciers are distributed over the Western, Southern and Central Alps. For each of the 6 glaciers a Landsat 8 or Sentinel-2 image was selected, which was then digitized by hand, independent of the implemented classification method. Within the RGI outline the snow areas were vectorized and assigned to category 1 (snow) and category 0 (no snow). The same images were also classified with our classifier. No hill shadow layer was added (c.f. chapter 4.2.2), as this would have made the classification of glaciers 4 and 6 obsolete, as they were completely shaded.

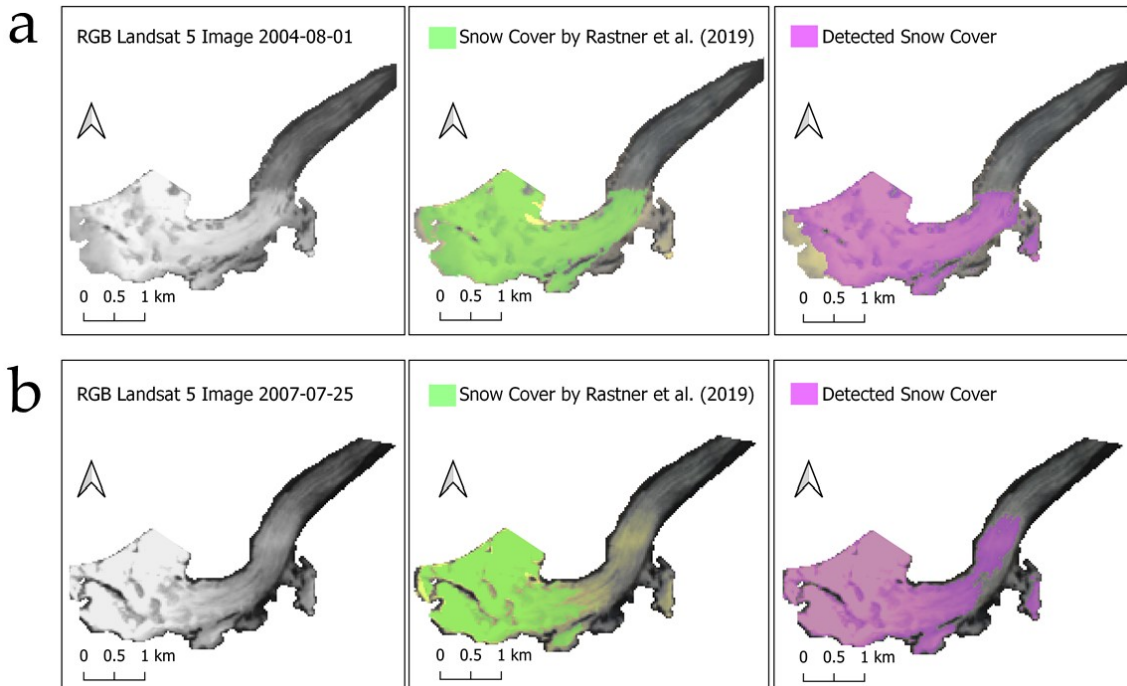


FIGURE 5.2: These two triplets show two scenes from 2004 and 2007 where there are major differences between Rastner et al. (2019) results and the results of this thesis. In 5.2a, the difference can be seen in the west. There are clouds here that Rastner et al. (2019) classified as snow. Our classifier did not classify the clouds as snow (but as clouds). However, in the area of the snow line in the lower part of the glacier no big differences can be seen.

In 5.2b there is a distinct difference in the area of the snow line. Rastner et al., 2019 classification is based directly on the determined Otsu-Threshold. In our classification, the area classified as ice is additionally analysed again using the brightness in the RGB bands. Bright pixels are then reassigned to the snow class (see chapter 4)

An example can be seen in figure 5.3, where the RGI outline, the manually digitized snow line and the snow cover classified by us are shown. To compare the vectorized reference data with the results of the classification, a rasterization had to be carried out. For the Landsat images to a pixel size of 30 m, for the two Sentinel-2 images with 20 m. This rasterization leads to a reduction in the accuracy of the reference data, which in turn leads to uncertainties in the results. The images we classified with up to 7 classes were also divided into two categories (snow and non-snow) in order to focus on the snow surfaces during validation. On the basis of the rasterized pixel maps of the hand-drawn snow areas and the snow areas of the classification, we have created a confusion matrix for each glacier. The results of the classification are summarized in table 5.2.

To quantify the reliability of the classification, the Cohen's Kappa (subsequently Kappa) according to Cohen (1960) is given for each image. This statistical measure shows how closely the datasets to be compared agree. A Kappa of 0 means that the agreement is random, which corresponds to a futile classification. A value of 1 indicates a perfect match. Table 5.1 according to Landis and Koch (1977) groups the kappa values into different categories for interpretation.

Glaciers 5, 6, 7 and 8 have different key indicators, but independently of the sensor (Landsat 8 or Sentinel-2) they achieved a kappa in the classification, which according to Landis and Koch

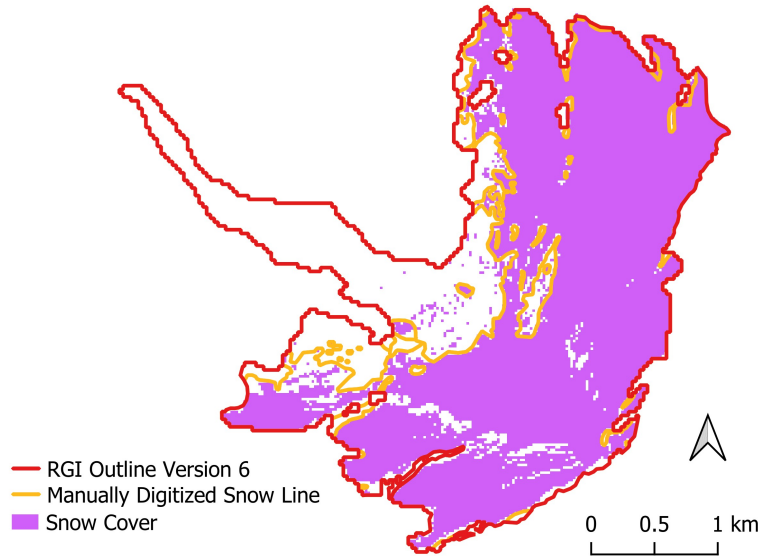


FIGURE 5.3: Comparison of the manually digitized snow line of the Oberer Grindelwaldgletscher (Glacier 8 in table 2.1) with the snow cover we classified. The classification achieved a Kappa of 0.778 and an Overall Accuracy (OA) of 92.11 %.

TABLE 5.1: The table shows the allocation of the Cohen’s Kappa (c.f. Cohen (1960)) values according to Landis and Koch (1977)

Kappa Value	Strength of Agreement
<0.00	Poor
0.00–0.20	Slight
0.21–0.40	Fair
0.41–0.60	Moderate
0.61–0.80	Substantial
0.81–1.00	Almost Perfect

(1977) definition represents a *substantial* agreement. Even though the number of glaciers tested is small, the kappa values are always high despite different preconditions (e.g. exposure, size, debris cover). Glacier 4 has a very low kappa value, which declares the classification as obsolete. For glacier 4, the Otsu value was 0.3, which is outside the given tolerance range. For this reason the snow and ice classification was made with the fixed value of 0.47 (c.f. chapter 4) Glacier 6 is larger than Glacier 4 and reached a Kappa of 0.386 in the validation, which is a *fair* agreement of the classifications (c.f. table 5.1). The achieved overall accuracy of 86.35 % is also considerably higher than that of Glacier 4.

## 5.2 Validation of the SLA and SCR Extraction

Two independent datasets are used to validate the extraction of the Snow Line Altitude (SLA) and the Snow Cover Ratio (SCR). For the validation of the SCR three glaciers from the target area are used (see table 2.1, Glacier 1 - 3). For the validation of the SLA extraction, a data series with 44 manually determined SLA values from the Abramov glacier in Kyrgyzstan is used (Barandun et al., 2015). These two parts are the structure of this section.

TABLE 5.2: Results of the classification validation for six alpine glaciers outside the target area. A visually classified map is compared with the automatic classification. The glacier numbers in the first column refer to table 2.1. The table shows the Producers Accuracy (PA) and the User Accuracy (UA) for the snow category. The Overall Accuracy (OA) refers to the accuracy of both categories. The Kappa Value is a measure of the strength of agreement between the visually classified map and the automatic classification (c.f. table 5.1).

Reference Glacier	GLIMS-ID	Sensor	Date	PA Snow	UA Snow	OA	Kappa's
4	G006799E45819N	Landsat 8	2015-06-18	95.14 %	64.43 %	71.30 %	0.072
6	G012249E47078N	Landsat 8	2015-06-06	80.71 %	90.97 %	86.35 %	0.386
5	G006846E45813N	Landsat 8	2015-07-20	78.22 %	99.31 %	88.84 %	0.772
7	G007898E45942N	Sentinel-2	2019-06-29	72.24 %	98.94 %	85.73 %	0.656
8	G008119E46614N	Landsat 8	2015-07-30	90.36 %	93.64 %	92.11 %	0.778
9	G010590E46392N	Sentinel-2	2015-07-04	98.86 %	74.37 %	82.40 %	0.717

### 5.2.1 Snow Cover Ratio Extraction

The basis for the validation of the SCR is provided by 16 measuring points from three glaciers in the Ötztal Alps, which were surveyed by Rastner et al. (2019). These data points are based on Landsat images from 1990 to 2011, whereby four of these images are also part of the classification analysis (see Chapter 5.1.1).

In figure 5.4 the Main Patches approach and the Altitude Bin approach are compared with the SCR data by Rastner et al. (2019). The obtained  $R^2$  values for the Main Patches approach are between 0.72 and 0.86. Those of the Altitude Bin approach are between 0.68 and 0.82. The comparison of the data must, however, be contextualised. The validation data were collected using manually checked glacier outlines from 2011. All our data was calculated with the RGI outlines of version 6. However, this difference cannot be quantified with this validation method.

### 5.2.2 Snow Line Altitude Extraction

Barandun et al. (2017) manually determined SLA values for the Abramov glacier in Kyrgyzstan (see table 2.1). Using Landsat 7 and 8 images, 44 data points were collected between 2003 and 2015. The satellite images show a low to non-existent cloud cover. To compare the three approaches, we used these 44 data points. One of these 44 classified images is shown in Figure 4.8. Figure 5.5 shows the results for each of the three approaches. On the X-axis is the manually determined SLA and on the Y-axis the corresponding point of the extraction method. The dotted line shows the linear regression line.

With a  $R^2$  of 0.92 the Altitude Bin approach (see figure 5.5a) shows the highest correlation. The root mean square error (RMSE) is about 50 m. Larger deviations are more likely to be found in the lower half of the altitude values. A slight accumulation of deviations can be seen in the middle range. However, this can probably be explained by the relative accumulation of data points in this altitude range. The stepped SLA results are clearly visible in the Altitude Bin approach. For this analysis a bin height of 50 m was used.

Figure 5.5b shows the results of the Main Patch approach. Here the  $R^2$  value is only slightly lower at 0.91. Notice the 4 lowest points on both axes where the Y-value at all four points is 3662 masl. This can be explained by the rules listed in table 4.2, which sets the lowest possible SLA for the



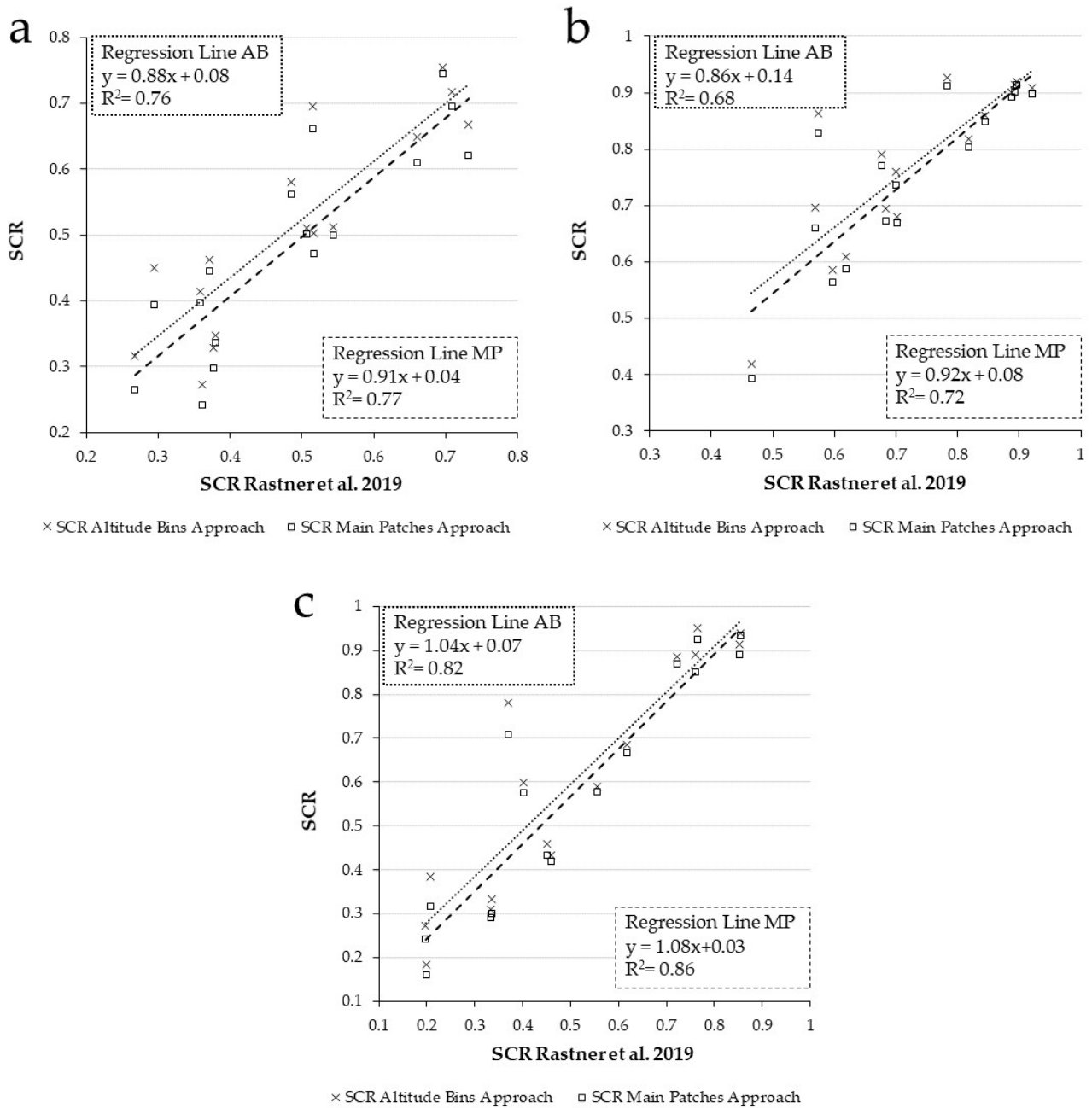


FIGURE 5.4: Comparison of the SCR values by Rastner et al. (2019) with the results of the Main Patch approach and Altitude Bin approach. 5.4a shows the values for the Hintereisferner, 5.4b for the Kesselwandferner and 5.4c the comparison with the data from the Vernagtferner. The higher values of the Altitude Bin approach (AB) compared to the Main Patch approach (MP) can be explained by a different methodology for deriving the values.

The  $R^2$  values are between 0.68 and 0.82, with the Main Patches approach values being slightly higher. The higher values of the Altitude Bin approach are based on a slightly different method, which assigns non-snow and non-ice area proportionally to the two classes. The partly clear differences to the validation data can also be explained by the different classification approach and the different glacier outlines used.

Main Patches approach when 95 % of the glacier surface is covered with snow.

The  $R^2$  of the Histogram approach is significantly lower than the other two approaches. There is no dispersion, especially for SLA values in the lower half of the data points. Due to the implemented

TABLE 5.3: Comparison of the  $R^2$  and RMSE data of the three approaches from the comparison with the visually determined SLA data from the Abramov glacier.

Comparison Data	$R^2$	RMSE	$R^2$ weighted	RMSE weighted
Alitude Bins SLA vs. Visual SLA	0.92	41.12	0.95	31.33
Main Patches SLA vs. Visual SLA	0.91	49.15	0.93	40.03
Histogram SLA vs. Visual SLA	0.68	117.43	0.67	108.60

rules, the values were set to the lowest possible SLA at a snow coverage of  $>90\%$  (c.f. table 4.3). There is a clear outlier (marked with an arrow in figure 5.5c. The error in the Histogram approach can be explained by a cloud and its shadow, which are only classified at the glacier margin, but lead to an error in the SLA determination.

In addition to the SLA, the snow and ice coverage is extracted for each image. The proportion of non-snow and non-ice can be used as a weighting for the quality of the corresponding SLA value. As a weighting for the 44 SLA values of the Abramov glacier, the non-snow and non-ice area (*void*) was determined for each image and scaled with the following formula:

$$1 + [(void - \min(void)) / (\max(void) - \min(void))] * -1$$

If these weights are used for the corresponding SLA values, the Altitude Bin approach and the Main Patches approach increase the  $R^2$  value by 0.03 and 0.02 respectively (see table 5.3).

### 5.2.3 Comparison with ELA and AAR-Data from the WGMS

The high and easy availability of satellite images as well as the steadily increasing temporal resolution can be used to investigate the course of the ablation period of a glacier. Through precise monitoring, the maximum snow line altitude (SLA), the minimum snow cover ratio (SCR) and thus the end of the ablation period can be determined (c.f. Yuwei et al., 2014).

For the three glaciers of the target area in the Ötztal Alps we have created time series with SLA and SCR data for the period 2015 to 2019 (filtered from 100 to 275 day of year) using the Main Patches approach and the Altitude Bin approach. The data tables of the plotted time series can be found in the Appendix (chapter 8). Figure 5.6 show the ablation period from 2015 to 2019 using the Vernagtferner (Glacier 2, Table 2.1) as an example. A total of 134 images from Vernagtferner with a cloud cover of  $<30\%$  were evaluated. A comparison with the ELA values of the WGMS is difficult. Where available, the ELA (Equilibrium Line Altitude) values from the WGMS are plotted with a dashed line. For the period from 2015 to 2019 there is only one ELA value for the Hintereisferner, for the Kesselwandferner there is no value reported. Due to the survey system of the WGMS (c.f. Kaser et al., 2003) it's not possible to assign the ELA to a specific date, so we plot it as a line in the corresponding ablation period. The data availability for the Accumulation Area Ratio (AAR) values at WGMS for the glaciers in the target area is poor. Figure 5.7 shows the snow cover ratio of the Kesselwandferner for the years 2015 to 2019. The dotted lines show the AAR values for the corresponding ablation periods. For the year 2019 no AAR data are available at WGMS. A total of 155 images from Kesselwandferner with a cloud cover of  $<30\%$  were evaluated.

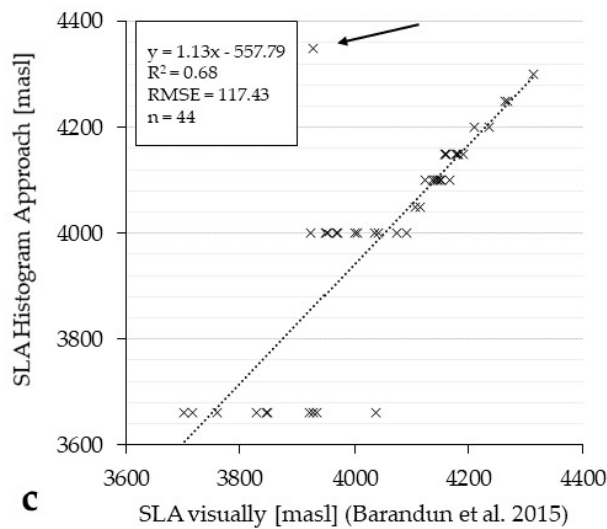
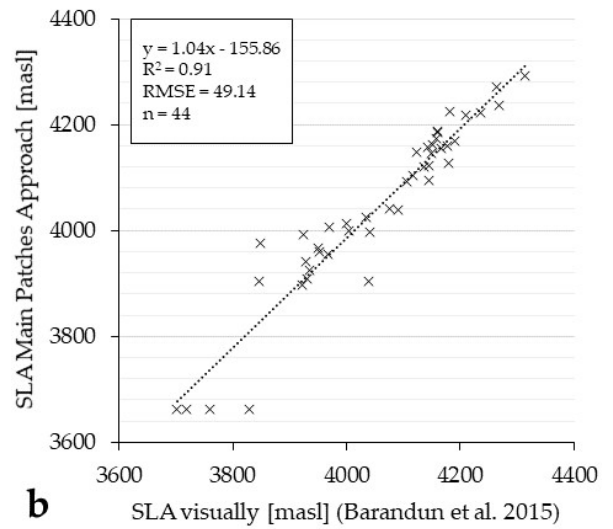
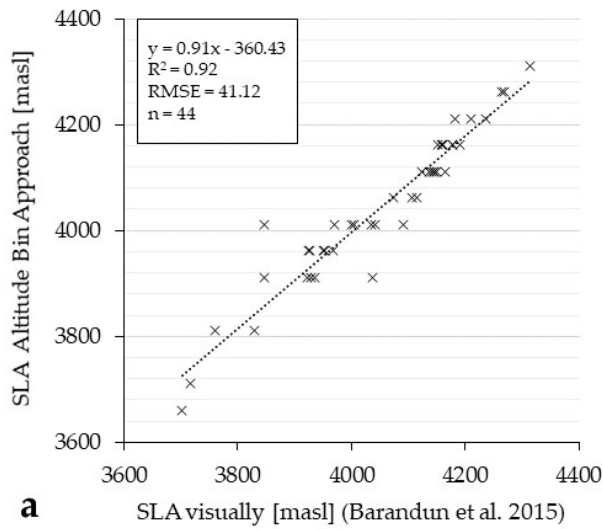


FIGURE 5.5: The graphs show the results of the SLA comparison between the three approaches and the 44 visually recorded SLA values by Barandun et al. (2015). Larger differences are particularly evident in the lower range of SLA values. These values are caused by the implemented rules that govern the handling of scenes with very high and very low snow cover.

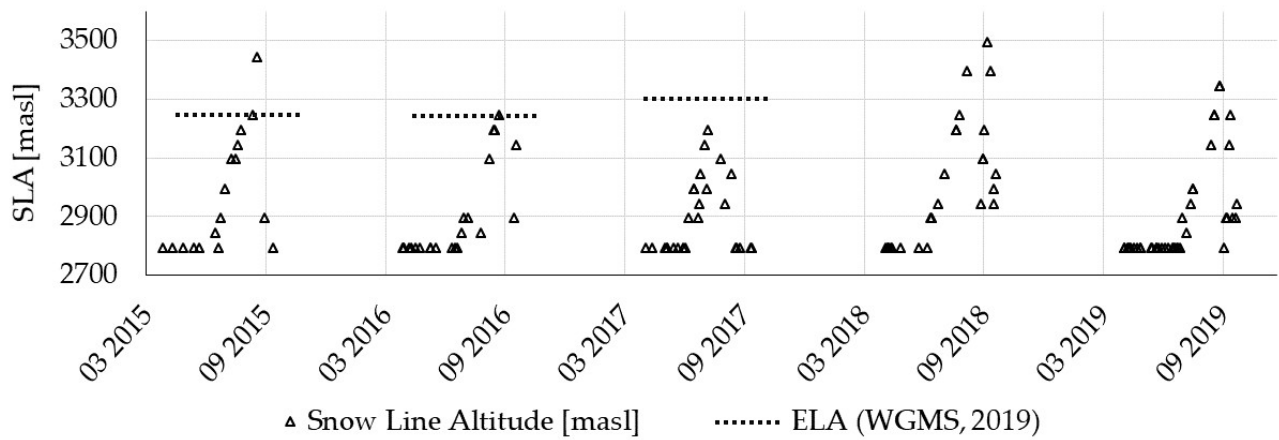


FIGURE 5.6: Snow Line Altitude (SLA) for the ablation periods 2015 to 2019 from Vernagtferner ( $n = 134$ ). The values were extracted using the Altitude Bin approach. The Equilibrium Line Altitude (ELA) values are from WGMS, no value is available for the year 2018 and 2019.

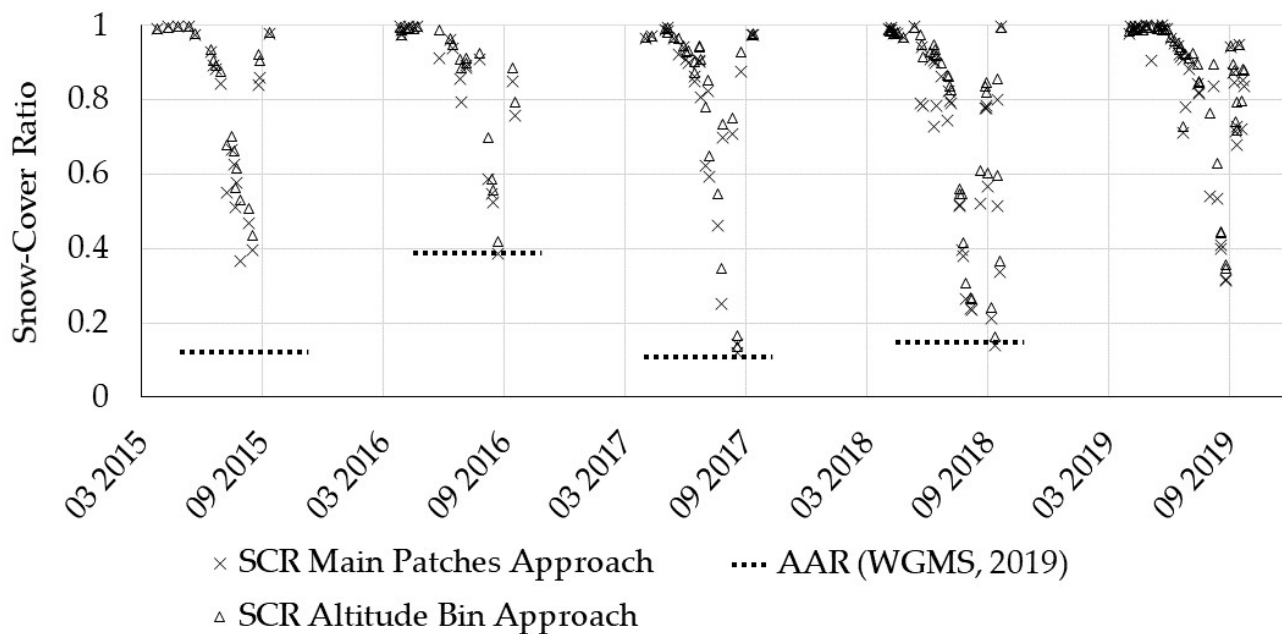


FIGURE 5.7: Snow Cover Ratio (SCR) for the ablation periods 2015 to 2019 from Kesselwandferner ( $n = 155$ ). The AAR-Values are from the WGMS indicate the AAR at the end of the balance year.



## 6 Discussion

### 6.1 Classification of glacial surface facies

#### 6.1.1 Accuracy of the classification

Two research questions of this thesis focus on the classification of glacier surfaces. The validation of the classification of glacier surfaces is difficult. The surfaces change considerably and due to the highly seasonal dependence of the snow cover, comparisons within one year are not possible. Precisely classified validation maps are not available, probably because the contours and surface classes are continuously changing. In this thesis we have worked with glacier outlines from 2003 (Abramov: 2000). For example, deviations of a few years have shown that the surface class *debris cover* is used for the exposed bedrock due to the retreat of the glaciers. In a narrower sense, such areas are no longer part of the glacier. But in order to have a comparable basis, the size of the glacier has to remain the same and only one glacier outline dataset is used for the whole process. The classification of surface classes other than snow and ice is becoming increasingly important in this sense. If one also takes the development of the improved spatial resolution into account, the mapping of additional classes becomes more and more important as well.

Depending on the analysis, a classified image can be used to monitor changes in length, glacier termini and the formation of lakes and streams on its surface or directly at the glacier terminus. The validation of our results with already existing snow cover maps and with 6 independent, visually collected reference data has shown that it's important to include several surface classes in the classification.

The qualitative comparison with existing snow cover maps shows that the classifier recognizes and classifies snow as such. Differences to existing approaches can be seen especially where our classifier recognizes and classifies additional surface types as snow and non-snow (like clouds or debris cover).

Clouds are not fundamentally a problem for determining the SLA. Depending on the method of extraction, non-snow and non-ice classes have a higher or lower influence. In the following chapter 6.2, the limitations of the approaches are discussed. The reclassification we proposed from very bright ice to the snow class could not be validated within the scope of this thesis but should be further investigated, including a distinction between ice, snow and firn.

In a direct comparison of the snow class of our classifier with the visually collected data, Kappa

values of 0.656 and 0.778 were obtained for glaciers  $<2.5 \text{ km}^2$ . These values show that a precise classification of snow on glaciers is possible. For the two glaciers  $>2.5 \text{ km}^2$ , in addition, both are north-exposed and steep, the classification of the surface is not feasible with the classifier presented here. Although shadow can be classified as such, the remaining area of snow and/or ice is not sufficient to derive a functional Otsu value. Therefore, if the fixed threshold is used, misclassifications result due to the shadow-prone location. For the validation data used (visual classification) the small-scale snow distribution in combination with a spatial resolution of 30m per pixel is also challenging.

Apart of steep and heavily shaded glaciers our program can be used. An optional hill shadow mask is implemented, which models and classifies hill shadows with the illumination of the sun and a DEM. Nevertheless, we assume that the lower limit of the applicability of the method presented in this thesis lies in the area size of approximately  $2.5 \text{ km}^2$ .

The improvement on the  $R^2$  values in SLA validation due to the weighting of the SLA values show that the non-snow and non ice surface also has an influence on the quality of the SLA extraction. For the experimental weighting a min-max scaling of the non-snow and non-ice area was used. This underlines the importance of defining and classifying different surface classes as precisely as possible.

The findings on classification of this thesis can be briefly summarised. For glaciers with an area  $>2.5 \text{ km}^2$  good classification results can be achieved (kappa of 0.656 to 0.778). A detailed classification with different surface classes such as debris cover or clouds can be used to refine the area that is important for the SLA and SCR and it's possible to extract good key indicators from the classified images.

Compared to other papers investigating the SLA extraction as a proxy for ELA, our method has the advantage that it can be used worldwide (c.f. Yuwei et al., 2014 or Mernild et al., 2013). The method presented in this thesis has the advantage over the thesis of Rastner et al. (2019) and Geibel (2019), that there is no need for time-consuming preparation of the data. In addition, the combination of Landsat and Sentinel-2 images makes it possible to create long time series (back to 1984) and to use the high temporal resolution available since 2016 to determine the end-of-summer SLA.

### **6.1.2 Random Forest Classifier**

Due to the high number of training points (100 points per class) that are set to train the Random Forest classifier, the images reclassified with Random Forest only differ minimal from the training image. Therefore, we have decided against a validation of the images. However, the approach to create a training dataset with a Decision Tree classifier has potential. We showed that it's possible to create a training dataset for a single glacier and then use it for all images of this glacier.

In the scope of this thesis the Random Forest classifier was only used for re-classification and it has been shown that this idea is feasible. Therefore, the decision tree classifier presented in this thesis

can be ideally used as a basis to create very large training datasets that are adapted to different sensors, geographical regions and seasonal changes.

## 6.2 Snow Line Altitude and Snow Cover Ratio Extraction

The third research question clarifies with which approach the SLA can be extracted from the classified images. In the scope of this thesis we have developed three approaches and implemented them in our program. The three approaches work independently of each other and are therefore discussed separately.

The comparison with the SLA data by Barandun et al. (2015) from the Abramov glacier shows that the Main Patches approach and the Altitude Bin approach with an  $R^2$  of 0.91 and 0.92 respectively achieve very good results. The Histogram approach with an  $R^2$  of 0.68 is clearly behind the other two. In comparison with Rastner et al.'s (2019) ASMAG, we achieved better results with the Main Patches approach and the Altitude Bin approach. However, it cannot be concluded whether this is due to the SLA extraction method or to the improved classification of the snow cover. It's interesting to note that the less non-snow and non-ice occurs on the glacier, the better our extraction works (Weighting of the SLA-values, see 5). This shows that clouds, debris cover or water have an impact on the accuracy of the SLA extraction. As already mentioned in the first part of the discussion, this shows that it is important not only to divide the glacier surfaces into two classes, but also to use additional surface facies. The date of outline determination also influences the accuracy. The changes in glacier length and volume resulting from climate change must be ensured by regularly updating the dataset. When classifying the surface within the RGI outlines, it's therefore important that different classes are considered, for example, to be able to classify newly formed surfaces in the glacier foreland.

The Histogram approach is sensitive to small-scale surface variations such as single snow patches below the SLA. The geometry of the glacier also has a major influence on successful SLA extraction. The method of minimizing the area difference and maximizing the total area at the corresponding altitude level means that areas on the glacier tongue are inferior to the normally larger accumulation area due to their narrow shape. This can lead to a wrong extraction of the SLA by an ice field in the comparatively larger accumulation area.

The Main Patches approach works best when there are two clearly visible main areas of snow and ice that are adjacent to each other. Calculating the median of the height values of the adjacent zone allows to determine a robust value of the SLA based on the used DEM. However, the rules for determining the SLA in situations where the surfaces do not touch, show clear weaknesses and can lead to outliers.

With the Altitude Bin approach, an SLA is determined with the snow proportion per altitude level. This method is more robust than the other two approaches, as three successive height levels are considered in each step. The partitioning of the height levels is completely flexible. Due to the inaccuracies and time differences between the DEM used and the SLA to be extracted, we use a step height of 50 m.



The further development of the Main Patch approach is especially interesting for determining the SLA with current and future images. If the spatial resolution of the images increases and additionally up-to-date DEM can be used, this approach offers the possibility to extract SLA values very accurately. For the analysis of already existing image datasets as well as for the creation of time series, the Altitude Bin approach offers robust results that also work at low spatial resolution.

With the Main Patches approach and the Altitude Bin approach, SCR values can also be extracted. The SCR validation values obtained are good, but need to be contextualised. The SCR values of Rastner et al. (2019) are based on a two-class classification (snow and no-snow). Differences in the classification are also explained in the first part of this chapter. For example, Figure 5.2a shows that in Rastner et al. (2019) clouds are assigned to the snow class. This leads to the result that, in such a case, the SCR values determined by us are lower than the validation values.

It's also important to note that the Altitude Bin approach values are always higher than the Main Patches values. As described in chapter 4, the SCR of the Altitude Bin approach is an approximation. To arrive at this value, the part classified as non-snow and non-ice is allocated proportionally between the two classes. This approximation is suitable, for example, when clouds cover a part of the glacier. With the proportional distribution, a cloud over the snow-covered area can be assigned to the snow class. This allocation increases the SCR value depending on the proportion of clouds, debris cover, water or shadow in the corresponding altitude level.

With the validation data used in this thesis it's not possible to identify which method is more suitable for determining the SCR. Although the  $R^2$  values of the Main patches approach are slightly higher, it should be mentioned again that Rastner et al. (2019) only work with a two-class classification of glacier surfaces, which, as mentioned, has an unquantifiable influence.

### 6.3 DEM Selection and Systematic Bias

In this thesis we use the ALOS-DEM with a spatial resolution of 30 m. In addition to the freely available DEM (see table 3.2), there are also commercially distributed DEM, some of which are very accurate (e.g. spatial resolution of 0.5 m with a vertical absolute accuracy of 3 m and 1 m relative accuracy with the Vicon DSM-0.5 (Prioretto et al., 2017, Schumann and Bates, 2018)).

The accuracy of SLA extraction can be improved in two ways. (1) It's well applicable to use a high-resolution DEM for SLA extraction. Such a DEM can only be available locally or a globally available high-resolution DEM is implemented. (2) An improvement of the data quality by using DEMs closer in time to the date the satellite image should also be examined. However, the benefits must be weighed up against the additional processing effort. The influence of the DEM on the SLA extraction is explained in the next part.

By using a DEM based on measurements from one year, there is a systematic bias in the extraction of the SLA, but also in the calculation of the topographic shadows. The already mentioned mass loss of glacier ice leads in most cases to a decrease in surface altitude. This effect depends on the mass loss, the volume distribution and the general bed topography of the glacier. In principle, it can be assumed that the tongue areas of glaciers are more affected by this effect. Rastner et al. (2019) examined this effect and compared three DEM from different points in time. Besides the suggestion to calculate a correction factor with DEM from three points in time and thus to adjust

the extracted SLA every year, they also point out that at the end of the ablation period the SLA to be extracted is located in the upper part of the glaciers, where the influence of the bias is typically smaller. Rastner et al. (2019) compared three DEM of the Hintereisferner (see table 2.1) of 1992, 2000 and 2013, using the SRTM DEM of 2000 as a reference. The deviations in the tongue area were +/- 60 m each. In the area of the mean height of the glacier (2800 m to 2900 m) the difference was +32 m (1992) and -21 m (2013). Comparing these values with the RMSE values calculated by our program when comparing them with manually obtained SLA values at the Abramov glacier, the values for two of the three methods are within this range (c.f. table 5.3). When analysing trends, this bias must be taken into account in particular and a more detailed analysis of the DEM differences must be carried out.

## **6.4 Monitor the SLA und SCR with a high temporal resolution**

The direct comparison from our SLA and SCR data with the WGMS bulletin-data showed, that our data can help to close existing data gaps and provide approximations for the ELA and AAR before they can be matched with conventional mass balance measurements. For the years from 2016 onwards, the SCR in particular correspond to the AAR values of the WGMS. For the year 2015, it should be noted that at the time of the ablation period, the Sentinel-2 satellite pair was not yet operational and has only been taking images with full temporal resolution since March 2016.

With our program it is possible to determine the maximum SLA and the minimum SCR in an automated way directly after the release of a new satellite image. Because there is no dependence on other data, our automated type of monitoring the snow cover on glaciers can be used easy, rapidly and worldwide.



## 7 Conclusion

With this thesis, we could show that a complete processing chain can be implemented in the GEE framework. Our program uses freely available data and can be used for the investigation of glaciers worldwide. The individual steps, which are executed in the code for monitoring the snow line altitude, are modular. This makes it possible to evaluate, improve, or expand individual steps even more precisely. The main findings of this work are summarised in the following points:

- A robust classifier, which performs under varying topographic and illumination conditions using a mix of fixed and variable thresholds, builds a solid foundation for further analysis.
- Next to snow and ice, other glacier surface fascias are also included in this classification. This comprehensive classification of glacier surfaces compensates for outdated glacier outlines which typically result in increased debris cover and glacial lakes. By classifying these areas, it is possible to focus on the snow and ice areas, since these areas most relevant for SLA extraction.
- The classification of the snow-ice mask in our classifier is based on an Otsu threshold on the NIR band. With the introduced classifier, kappa values between 0.656 and 0.778 could be achieved, which corresponds to a substantial agreement with the visually collected data from independently selected glaciers in the Alps.
- Three approaches were developed and evaluated for the extraction of the SLA. The Histogram approach and the Altitude Bin approach are based on the distribution of the snow and ice classes per altitude level. The Main Patches approach uses the direct border of the main snow and ice classes. Promising  $R^2$  values were achieved with the Main Patches approach (0.91) and the Altitude Bin approach (0.92). A comparably low performance with a  $R^2$  of 0.68 resulted from the Histogram approach.
- The Main Patches approach and the Altitude Bin approach are furthermore capable to extract the snow cover ratio. The Main Patches approach directly compares the area classified as snow with the total area of the glacier. The Altitude Bin approach allocates the area classified as non-snow and non-ice to the snow and ice classes proportionately at each altitude level.

The SCR values of the Main Patches approach performed slightly better (R2 difference of 0.03 onm the average) when comparing the two approaches.

- With the highly increased data availability by the Sentinel-2 constellation, it is possible to visualize the course of the ablation period of glaciers using the SCR and the SLA. Our program offers a interesting possibility to close existing data gaps which exist for instance in the WGMS database. Such data gaps arise because determining ELA with photogrammetric and ground-based methods is time-consuming and expensive. Our method offers the possibility to create proxies for the ELA worldwide, if satellite images are available.

The encouraging results achieved with the classifier presented in this thesis and two developed SLA extraction approaches offers a wide field for further research. Three options for follow-up research are listed below:

- This thesis shows that the decision tree classifier presented can be used to efficiently create large training datasets for a random forest classifier. The use of further AI-based classifiers or a connection to the TensorFlow-framework are conceivable. With our decision tree classifier, individual training datasets can be created. It's also possible to create sensor-specific, regional or global training data.
- The use of freely available data with global coverage makes it possible to study glaciers globally. The modular structure of the program also enables the use of additional approaches. With few adjustments in the processing chain, it's also conceivable to calculate reference datasets for larger areas in order to use the data as an approximation of the mass balance.
- By implementing the fully automated analysis process in the GEE framework, a broad use of such a tool can be promoted. The simple GUI makes it easy to extract the required data and create data for a further analyses. First independent users of the application expressed interest and expect a great benefit from this easy-to-use way of generating data. Easy access to remotely sensed data for glaciology helps to promote interdisciplinary research and allows scientific findings to be transferred quickly from one field of research to another.

## Bibliography

- Barandun, M., M. Huss, L. Sold, D. Farinotti, E. Azisov, N. Salzmann, R. Usabaliev, A. Merkushkin, and M. Hoelzle (2015). "Re-analysis of seasonal mass balance at Abramov glacier 1968-2014." *Journal of Glaciology* 61.230, pp. 1103–1117.
- Barandun, M., M. Huss, E. Berthier, A. Käab, E. Azisov, T. Bolch, R. Usabaliev, and M. Hoelzle (2017). "Multi-decadal mass balance series of three Kyrgyz glaciers inferred from transient snowline observations." *The Cryosphere Discussions*.
- Breiman, L. (2001). "Random Forests." *Machine Learning* 45.1, pp. 5–32.
- Chander, G., B. L. Markham, and D. L. Helder (2009). "Summary of current radiometric calibration coefficients for Landsat MSS, TM, ETM+, and EO-1 ALI sensors." *Remote Sensing of Environment* 113.5, pp. 893–903.
- Cogley, J. G. (2009). "Geodetic and direct mass-balance measurements: Comparison and joint analysis." *Annals of Glaciology* 50.50, pp. 96–100.
- Cohen, J. (1960). "A Coefficient of Agreement for Nominal Scales." *Educational and Psychological Measurement* 20.1, pp. 37–46.
- Cuffey, K. and W. Paterson (2010). *The Physics of Glaciers*. Vol. Fourth edi. Amsterdam.
- Donchyts, G. (2016). *Basic Cloud Shadow Shift*.
- ESA (2015). *Sentinel-2 User Handbook*.
- Farr, T. G., P. A. Rosen, E. Caro, R. Crippen, R. Duren, S. Hensley, M. Kobrick, M. Paller, E. Rodriguez, L. Roth, D. Seal, S. Shaffer, J. Shimada, J. Umland, M. Werner, M. Oskin, D. Burbank, and D. E. Alsdorf (2007). "The shuttle radar topography mission." *Reviews of Geophysics* 45.2.
- Furbish, D. J. and J. T. Andrews (1984). "The use of hypsometry to indicate long-term stability and response of valley glaciers to changes in mass transfer." *Journal of Glaciology* 30.105, pp. 199–211.
- Geibel, L. (2019). "SnowIceSen": An Automated Tool to Map Snow and Ice on Glaciers with Sentinel-2.
- Gorelick, N., M. Hancher, M. Dixon, S. Ilyushchenko, D. Thau, and R. Moore (Dec. 2017). "Google Earth Engine: Planetary-scale geospatial analysis for everyone." *Remote Sensing of Environment* 202, pp. 18–27.
- Hall, D. K. and G. A. Riggs (2010). "Normalized-Difference Snow Index (NDSI)." *Encyclopedia of Snow, Ice and Glaciers*.
- Huggel, C., A. Käab, W. Haeberli, P. Teysseire, and F. Paul (2002). "Remote sensing based assessment of hazards from glacier lake outbursts: A case study in the Swiss Alps." *Canadian Geotechnical Journal* 39.2, pp. 316–330.

- Huss, M, B Bookhagen, C Huggel, D Jacobsen, R. S. Bradley, J. J. Clague, M Vuille, W Buytaert, D. R. Cayan, G Greenwood, B. G. Mark, A. M. Milner, R Weingartner, and M Winder (2017). "Toward mountains without permanent snow and ice." *Earth's Future* 5, pp. 418–435.
- Immerzeel, W. W., A. F. Lutz, M. Andrade, A. Bahl, H. Biemans, T. Bolch, S. Hyde, S. Brumby, B. J. Davies, A. C. Elmore, A. Emmer, M. Feng, A. Fernández, U. Haritashya, J. S. Kargel, M. Koppes, P. D. Kraaijenbrink, A. V. Kulkarni, P. A. Mayewski, S. Nepal, P. Pacheco, T. H. Painter, F. Pellicciotti, H. Rajaram, S. Rupper, A. Sinisalo, A. B. Shrestha, D. Viviroli, Y. Wada, C. Xiao, T. Yao, and J. E. Baillie (Jan. 2020). "Importance and vulnerability of the world's water towers." *Nature* 577.7790, pp. 364–369.
- IPCC (2019). *Summary for Policymakers*. In press.
- JAXA (2017). "ALOS Global Digital Surface Model ( DSM ) " ALOS World 3D-30m " ( AW3D30 ) Dataset Product Format Description Earth Observation Research Center ( EORC ), Japan Aerospace Exploration Agency ( JAXA )." March, p. 11.
- Kääb, A., T. Bolch, K. Casey, T. Heid, J. S. Kargel, G. J. Leonard, F. Paul, and B. H. Raup (2014). "Glacier Mapping and Monitoring Using Multispectral Data." *Global Land Ice Measurements from Space*, pp. 75–112.
- Kaser, G., A. G. Fountain, and P. Jansson (2003). "A Manual for monitoring the mass balance of mountain glaciers with particular attention to low latitude characteristics; Technical documents in hydrology." *IHPVI Technical documents in Hydrology* 2003.59, pp. 1–137.
- Klug, C., E. Bollmann, S. P. Galos, L. Nicholson, R. Prinz, L. Rieg, R. Sailer, J. Stötter, and G. Kaser (2018). "Geodetic reanalysis of annual glaciological mass balances (2001-2011) of Hintereisferner, Austria." *Cryosphere* 12.3, pp. 833–849.
- Landis, J. R. and G. G. Koch (1977). "The Measurement of Observer Agreement for Categorical Data." *Biometrics* 33.1, pp. 159–174.
- Liang, S., C. J. Shuey, A. L. Russ, H. Fang, M. Chen, C. L. Walthall, C. S. Daughtry, and R. Hunt (2003). "Narrowband to broadband conversions of land surface albedo: I Algorithms." *Remote Sensing of Environment* 84.1, pp. 25–41.
- Martinuzzi, S., W. Gould, and O. González (2007). "Creating cloud-free Landsat ETM+ data sets in tropical landscapes: cloud and cloud-shadow removal." *General Technical Report IITF-GTR-32* December 2013, pp. 1–18.
- Medwedeff, W. G. and G. H. Roe (2017). "Trends and variability in the global dataset of glacier mass balance." *Climate Dynamics* 48.9-10, pp. 3085–3097.
- Mernild, S. H., M. Pelto, J. K. Malmros, J. C. Yde, N. T. Knudsen, and E. Hanna (2013). "Identification of snow ablation rate, ELA, AAR and net mass balance using transient snowline variations on two arctic glaciers." *Journal of Glaciology* 59.216, pp. 649–659.
- Naegeli, K., A. Damm, M. Huss, H. Wulf, M. Schaepman, and M. Hoelzle (2017). "Cross-Comparison of Albedo Products for Glacier Surfaces Derived from Airborne and Satellite (Sentinel-2 and Landsat 8) Optical Data." *Remote Sensing* 9.2, p. 110.
- Naegeli, K., M. Huss, and M. Hoelzle (2019). "Change detection of bare-ice albedo in the Swiss Alps." *Cryosphere* 13.1, pp. 397–412.
- Otsu, N. (1979). "Threshold Selection Method From Gray-Level Histograms." *IEEE Trans Syst Man Cybern* SMC-9.1, pp. 62–66.

- Paul, F., S. H. Winsvold, A. Käab, T. Nagler, and G. Schwaizer (2016). "Glacier remote sensing using Sentinel-2. part II: Mapping glacier extents and surface facies, and comparison to Landsat 8." *Remote Sensing* 8.7, pp. 0–15.
- Pfeffer, W. T., A. A. Arendt, A. Bliss, T. Bolch, J. G. Cogley, A. S. Gardner, J. O. Hagen, R. Hock, G. Kaser, C. Kienholz, E. S. Miles, G. Moholdt, N. Mölg, F. Paul, V. Radić, P. Rastner, B. H. Raup, J. Rich, M. J. Sharp, L. M. Andreassen, S. Bajracharya, N. E. Barrand, M. J. Beedle, E. Berthier, R. Bhambri, I. Brown, D. O. Burgess, E. W. Burgess, F. Cawkwell, T. Chinn, L. Copland, N. J. Cullen, B. Davies, H. De Angelis, A. G. Fountain, H. Frey, B. A. Giffen, N. F. Glasser, S. D. Gurney, W. Hagg, D. K. Hall, U. K. Haritashya, G. Hartmann, S. Herreid, I. Howat, H. Jiskoot, T. E. Khromova, A. Klein, J. Kohler, M. König, D. Kriegel, S. Kutuzov, I. Lavrentiev, R. Le Bris, X. Li, W. F. Manley, C. Mayer, B. Menounos, A. Mercer, P. Mool, A. Negrete, G. Nosenko, C. Nuth, A. Osmonov, R. Pettersson, A. Racoviteanu, R. Ranzi, M. A. Sarikaya, C. Schneider, O. Sigurdsson, P. Sirguey, C. R. Stokes, R. Wheate, G. J. Wolken, L. Z. Wu, and F. R. Wyatt (2014). "The Randolph glacier inventory: A globally complete inventory of glaciers." *Journal of Glaciology* 60.221, pp. 537–552.
- Pichler, M. and M. Pasquini (2009). "Das Klima im Ötztal." *Exkursionsführer Globaler Wandel LFU Innsbruck*. Ed. by C. Geitner and K. Scharr. Innsbruck.
- Prioretti, S., F. Lorenzon, A. Uttenthaler, A. Klaus, and M. Probeck (2017). *Overview of Global DEM Assessment of the current global DEMs and requirements for an updated global DEM*.
- Rabatel, A., J. P. Dedieu, and C. Vincent (2005). "Using remote-sensing data to determine equilibrium-line altitude and mass-balance time series: Validation on three French glaciers, 1994-2002." *Journal of Glaciology* 51.175, pp. 539–546.
- Rastner, P., R. Prinz, C. Notarnicola, L. Nicholson, R. Sailer, G. Schwaizer, and F. Paul (2019). "On the Automated Mapping of Snow Cover on Glaciers and Calculation of Snow Line Altitudes from Multi-Temporal Landsat Data." *Remote Sensing* 11.12, pp. 1–24.
- Rounce, D. R., C. S. Watson, and D. C. McKinney (2017). "Identification of hazard and risk for glacial lakes in the Nepal Himalaya using satellite imagery from 2000-2015." *Remote Sensing* 9.7.
- Schumann, G. J.-P. and P. D. Bates (2018). "The Need for a High-Accuracy, Open-Access Global DEM." *Frontiers in Earth Science* 6.December, pp. 1–5.
- Tachikawa, T., M. Kaku, A. Iwasaki, D. B. Gesch, M. J. Oimoen, Z. Zhang, J. J. Danielson, T. Krieger, B. Curtis, J. Haase, M. Abrams, and C. Carabajal (2011). *ASTER Global Digital Elevation Model Version 2 - summary of validation results*. Tech. rep.
- Takaku, J., T. Tadono, and K. Tsutsui (2014). "Generation of high resolution global DSM from ALOS PRISM." *International Archives of the Photogrammetry, Remote Sensing and Spatial Information Sciences - ISPRS Archives* 40.4, pp. 243–248.
- Waske, B., S. van der Linden, C. Oldenburg, B. Jakimow, A. Rabe, and P. Hostert (2012). "ImageRF - A user-oriented implementation for remote sensing image analysis with Random Forests." *Environmental Modelling and Software* 35, pp. 192–193.
- WGMS (2018). *Fluctuations of Glaciers Database*. World Glacier Monitoring Service, Zurich, Switzerland. URL: <http://dx.doi.org/10.5904/wgms-fog-2018-11>.
- Williams, R. S., D. K. Hall, and C. S. Benson (1991). "Analysis of glacier facies using satellite techniques." *Journal of Glaciology* 37.125, pp. 120–128.



- Yuwei, W. U., H. E. Jianqiao, G. Zhongming, and C. Anan (2014). "Limitations in identifying the equilibrium-line altitude from the optical remote-sensing derived snowline in the Tien Shan, China." *Journal of Glaciology* 60.224, pp. 1117–1125.
- Zemp, M., M. Huss, E. Thibert, N. Eckert, R. McNabb, J. Huber, M. Barandun, H. Machguth, S. U. Nussbaumer, I. Gärtner-Roer, L. Thomson, F. Paul, F. Maussion, S. Kutuzov, and J. G. Cogley (2019). "Global glacier mass changes and their contributions to sea-level rise from 1961 to 2016." *Nature* 568.7752, pp. 382–386.

## 8 Appendices

### 8.1 Code

The code can be accessed at `www.slamonitoring.josiaszeller.ch`.

For users of the Google Earth Engine, the repository can be accessed at `https://code.earthengine.google.com/?accept_repo=users/josiaszeller/Thesis`.

## 8.2 Data Tables

TABLE 8.1: Excerpt from the table with SCR and SLA from Kesselwandferner 2015 to 2019 - Results from the Main Patches Approach (MP) and the Altitude Bin Approach (AB)

system:index	Date	SCR MP	SLA MP	SCR AB	SLA AB	Void Ratio
1_1_2_LC08_193028_20150410	10.04.2015	0.993	2757	0.991	2757	0.000
1_1_2_LC08_193028_20150426	26.04.2015	0.996	2757	0.996	2757	0.000
1_1_2_LC08_193028_20150512	12.05.2015	0.999	2757	0.999	2757	0.000
1_1_2_LC08_193028_20150528	28.05.2015	0.998	2757	0.997	2757	0.000
1_1_1_2_LE07_193027_20150605	05.06.2015	0.975	2757	0.977	2907	0.005
1_1_2_LC08_193028_20150629	29.06.2015	0.929	2757	0.934	2957	0.029
1_2_20150704T101337_20160809T015434_T32TPS	04.07.2015	0.893	2964	0.906	2957	0.041
1_1_1_2_LE07_193027_20150707	07.07.2015	0.884	2997	0.892	2957	0.040
1_1_2_LC08_193028_20150715	15.07.2015	0.843	3048	0.876	3057	0.063
1_2_20150724T101006_20160815T201217_T32TPS	24.07.2015	0.549	3107	0.680	3107	0.423
1_1_2_LC08_193028_20150731	31.07.2015	0.666	3115	0.702	3107	0.085
1_2_20150803T101010_20160716T050046_T32TPS	03.08.2015	0.627	3124	0.661	3107	0.095
1_2_20150806T102012_20160721T205724_T32TPS	06.08.2015	0.512	3121	0.564	3157	0.192
1_1_1_2_LE07_193027_20150808	08.08.2015	0.576	3134	0.615	3157	0.093
1_2_20150813T101657_20160706T052644_T32TPS	13.08.2015	0.366	3131	0.532	3157	0.295
1_2_20150826T102655_20160711T192734_T32TPS	26.08.2015	0.469	3167	0.507	3157	0.112
1_1_2_LC08_193028_20150901	01.09.2015	0.396	3174	0.434	3157	0.119
1_1_1_2_LE07_193027_20150909	09.09.2015	0.842	2991	0.923	3007	0.112
1_2_20150912T101724_20160713T154341_T32TPS	12.09.2015	0.860	2963	0.907	2957	0.094
1_1_1_2_LE07_193027_20150925	25.09.2015	0.979	2757	0.981	2757	0.001

The complete table can be accessed at <https://bit.ly/2ZpG2DM>.

TABLE 8.2: Excerpt from the table with SCR and SLA from Vernagferner 2015 to 2019 - Results from the Main Patches Approach (MP) and the Altitude Bin Approach (AB)

system:index	Date	SCR MP	SLA MP	SCR AB	SLA AB	Void Ratio
1_1_2_LC08_193027_20150410	10.04.2015	0.990	2795	0.990	2795	0.000
1_1_2_LC08_193027_20150426	26.04.2015	0.998	2795	0.998	2795	0.000
1_1_2_LC08_193027_20150512	12.05.2015	1.000	2795	1.000	2795	0.000
1_1_2_LC08_193028_20150528	28.05.2015	0.908	2795	0.907	2795	0.000
1_1_1_2_LE07_193027_20150605	05.06.2015	0.962	2795	0.976	2795	0.015
1_1_2_LC08_193027_20150629	29.06.2015	0.960	2795	0.963	2845	0.003
1_2_20150704T101337_20160809T015434_T32TPT	04.07.2015	0.910	3386	0.940	2795	0.040
1_1_1_2_LE07_193027_20150707	07.07.2015	0.890	3094	0.921	2895	0.048
1_1_2_LC08_193027_20150715	15.07.2015	0.772	2997	0.811	2995	0.085
1_2_20150724T101006_20160815T201217_T32TPT	24.07.2015	0.414	3080	0.635	3095	0.454
1_1_2_LC08_193027_20150731	31.07.2015	0.449	3106	0.489	3095	0.132
1_2_20150803T101010_20160716T050046_T32TPT	03.08.2015	0.410	3125	0.456	3145	0.150
1_1_1_2_LE07_193027_20150808	08.08.2015	0.224	3176	0.340	3195	0.322
1_2_20150826T102655_20160711T192734_T32TPT	26.08.2015	0.245	3147	0.287	3245	0.185
1_1_2_LC08_193028_20150901	01.09.2015	0.126	3334	0.145	3445	0.200
1_2_20150912T101724_20160713T154341_T32TPT	12.09.2015	0.615	3163	0.867	2895	0.325
1_1_1_2_LE07_193027_20150925	25.09.2015	0.972	2795	0.974	2795	0.001
1_2_20160409T101141_20160409T154605_T32TPT	09.04.2016	0.996	2795	0.993	2795	0.000
1_1_2_LC08_193027_20160412	12.04.2016	0.985	2795	0.986	2795	0.001
1_2_20160412T102058_20160412T143526_T32TPT	12.04.2016	0.953	2795	0.969	2795	0.021

The complete table can be accessed at <https://bit.ly/2Zpg2DM>.



## Acknowledgements

I would first like to thank my two thesis advisors **Dr. Hendrik Wulf** and **Dr. Philipp Rastner** of the Department of Geography at the University of Zurich. The open and constructive exchange and their interest and motivation helped me to work on this thesis with enthusiasm. This thesis was written in the middle of a big stress test for all of us. The measures to combat COVID-19 affected us all and changed our lives from one day to the next.

Finally, I also thank my roommates with whom I spent this special time in the 'home-office'. Especially I must express my very profound gratitude to my parents and my girlfriend, for providing me continuous support and outstanding motivation throughout my years of study. All these experiences would not have been possible without your support. Thank you!

Stay healthy and safe.

Josias Zeller



## Personal Declaration

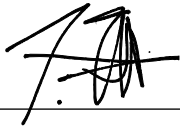
I hereby declare that the submitted thesis is the result of my own, independent work. All external sources are explicitly acknowledged in the thesis.

Date

June 30, 2020

Signature

Josias Zeller

A handwritten signature in black ink, appearing to be 'J. Zeller', written over a horizontal line.